THESIS

STRUCTURE AND ELECTRONIC PROPERTIES OF "DNA-GOLD-NANOTUBE" SYSTEMS: A QUANTUM CHEMICAL ANALYSIS

PANVIKA PANNOPARD

GRADUATE SCHOOL, KASETSART UNIVERSITY

2007

THESIS APPROVAL

GRADUATE SCHOOL, KASETSART UNIVERSITY

Master of Science (Chemistry)
DEGREE

Chemistry   Chemistry
FIELD   **DEPARTMENT**

TITLE: Structure and Electronic Properties of "DNA-Gold-Nanotube" Systems:
A Quantum Chemical Analysis

NAME: Miss Panvika Pannopard

THIS THESIS HAS BEEN ACCEPTED BY

_____ THESIS ADVISOR
(Mr. Tanin Nanok, Ph.D.   )

_____ COMMITTEE MEMBER
(Professor. Jumras Limtrakul, Ph.D.   )

_____ COMMITTEE MEMBER
(Miss Pensri Bunswansong, Ph.D   )

_____ DEPARTMENT HEAD
(Assistant Professor Noojaree Prasitpun, Ph.D.)

APPROVED BY THE GRADUATE SCHOOL ON   4|6|07

_____ DEAN
(Associate Professor Vinai Artkongharn, M. A.)

THESIS

STRUCTURE AND ELECTRONIC PROPERTIES OF "DNA-GOLD-NANOTUBE" SYSTEMS: A QUANTUM CHEMICAL ANALYSIS

PANVIKA PANNOPARD

A Thesis Submitted in Partial Fulfillment of

the Requirements for the Degree of

Master of Science (Chemistry)
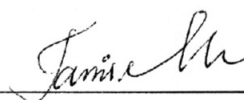
Graduate School, Kasetsart University

2007

Panvika Pannopard 2007: Structure and Electronic Properties of "DNA-Gold-Nanotube" Systems: A Quantum Chemical Analysis. Master of Science (Chemistry), Major Field: Chemistry, Department of Chemistry. Thesis Advisor: Mr. Tanin Nanok, Ph.D. 83 pages.

The development of a novel DNA sensor is a crucial issue in the diagnosis of pathogenic and genetic diseases. We used the Density Functional Theory (DFT) to investigate the DNA sensor performance of hybrid structures of a gold atom (Au) deposited on two types of single-walled carbon nanotubes: armchair SWCNT(8,0)/Au and zigzag SWCNT(5,5)/Au and compared these with bare Au. The adenine:thymine (A:T) complex is used to represent the base pair in the DNA double helix. The recognition probe is defined as SWCNT/Au/A in which an adenine molecule is immobilized on the SWCNT/Au supporter via its active N7 anchor point. After thymine hybridization (SWCNT/Au/A:T), the overall modulations are analyzed by comparing them with original systems. The hybrid systems, "SWNCTs/Au", exhibit good stability and sensitivity. This is originated from the co-function of a gold atom, which acts as a powerful electron withdrawing group, and SWNCTs, which act as electron collecting centers. With Mulliken population analysis, it was found that the "SWCNTs/Au" could accumulate the electron density better than the bare gold atom by, at most, four times when forming with the A:T complex. We also applied SWCNTs/Au complex as a sensing material for nucleic acids. The SWCNT/Au structure was more reactive to adenine capturing than the bare Au atom. Especially, the SWCNT(8,0)/Au/A system can accelerate target adenine electrons to the SWCNT(8,0)/Au sensing part. Another gold size which also be attached on both SWCNTs was a triangular gold cluster (Au_3). There are several binding characteristics between them, though the best stable complex of each SWCNT is SWCNT(8,0)/Au_3(ApU) (40.2 kcal/mol) and SWCNT(5,5)/Au_3(ApD) (29.9 kcal/mol). The monitoring of molecular charge modulations after the SWCNT/Au_3/A probe binds with the target thymine molecule infers that the sensing quality of SWCNT(8,0)/Au_3(ApU) and SWCNT(5,5)/Au_3(ApD) is better than the bare Au_3 cluster. The SWCNT(8,0) is more suitable to use as the SWCNT/Au_3 supporter than the SWCNT(5,5) due to its great affinity to Au_3 cluster. The overall results of "SWNCTs/Au" and "SWNCTs/Au_3" lead to the propose that the "SWCNTs/gold" systems could be the potential candidate for a nanostructure-based DNA sensor.

Panvika Pannopard	Jamie Nu	1 / 11 / 07
Student's signature	Thesis Advisor's signature	

ACKNOWLEDGEMENTS

TABLE OF CONTENTS

Page

LIST OF TABLES

LIST OF TABLES (Continued)

LIST OF FIGURES

LIST OF FIGURES (Continued)

LIST OF FIGURES (Continued)

LIST OF FIGURES (Continued)

LIST OF FIGURES (Continued)

LIST OF ABBREVIATIONS

A	=	Adenine
Å	=	Angstrom
a.u.	=	Atomic Unit
ALAx	=	Along Axis
ApD	=	Apex-Down
ApH	=	Apex-Hollow
ApH	=	Apex-Bond
ApT	=	Apex-Top
ApU	=	Apex-Up
Au	=	Gold
Au NPs	=	Gold Nanoparticles
B3LYP	=	Becke 3-Parameter (Exchange), Lee, Yang and Parr (Correlation); Density Functional Theory
BsB	=	Basal-Bond
BsH	=	Basal-Hollow
BsT	=	Basal-Top
C	=	Cytosine
C	=	Carbon
cc-pVDZ	=	Correlation Consistence Polarized Valence Double Zeta
cc-pVTZ	=	Correlation Consistence Polarized Valence Triple Zeta
CMOS	=	Complementary Metal-Oxide Semiconductor
CNTs	=	Carbon Nanotubes
DFT	=	Density Functional Theory
DNA	=	Deoxy-ribo Nucleic Acid
Eb	=	Binding Energy
ECP	=	Effective Core Potential
eV	=	Electron Volt

LIST OF ABBREVIATIONS (Continued)

G	=	Gaunine
H	=	Hydrogen
HRTEM	=	High-Resolution Transmission Electron Microscopy
IP	=	In Plane
kcal/mol	=	kilocalorie per mol
MCH	=	Mercaptohexanol
MWCNTs	=	Multiwall Carbon Nanotubes
N	=	Nitrogen
nm	=	Nanometer
O	=	Oxygen
PBE	=	Perdew, Burke and Ernzerhof
PDAx	=	Perpendicular Axis
PP	=	Perpendicular Plane
qm	=	Mulliken Charge
RECP	=	Relativistic Effective Core Potential
RI	=	Resolution of the Identity
$Ru(bpy)_3^{2+}$	=	Tris(2,2'-bipyridyl) ruthenium(II)
SWCNTs	=	Single-wall Carbon Nanotubes
T	=	Thymine
TDP	=	Temperature-Programmed Desorption
TEM	=	Transmission Electron Microscopy
UV-Vis	=	Ultraviolet Visible
WC	=	Watson-Crick

STRUCTURE AND ELECTRONIC PROPERTIES OF "DNA-GOLD-NANOTUBE" SYSTEMS: A QUANTUM CHEMICAL ANALYSIS

INTRODUCTION

The idea of chemical sensing based on molecular recognition is considered as one of the most promising concepts for single-molecule detection, even though it still remains in an early developmental stage. The approach requires probes which hold a specific recognition of desired chemical species and a transduction ability of that recognition incident into a quantitative response signal. Due to those indispensable functions, this concept is very versatile for the fabrication of a chemical sensing probe that integrates both recognition and transduction moieties into a single molecular assembly. The scheme has been examined in various disciplines, especially for a nature imitated detection of specific DNA sequences (Drummond et al., 2003; Vercoutere and Akeson, 2002; Wang, 2002; Zhai et al., 1997).

The exclusive properties of gold nanoparticles (Au NPs) are high sensitivity, electrical conductivity, size-dependent optical capability and affinity to the biomolecules (Daniel and Astruc, 2004; Natalia et al., 2006; Thaxton et al., 2006; Zhang et al., 2005). Integrating new capabilities for controlling particle size with versatile surface modification allows for the tailoring of optically and chemically encoded gold-nanoparticle probes. Over the past several years, there is an increasing interest to apply these probes in DNA detection devices. Several groups have developed powerful gold-nanoparticle-based DNA hybridization assays with numerous electrical detection strategies. Selected examples are shown in Figures 1, 2 and 3. Regarding the optical detection, Figure 1, (Thaxton *et al.*, 2006), the colorimetric hybridization signal is governed by the difference in optical properties of dispersed and aggregated gold nanoparticles. In DNA detection, Au nanoparticles are modified with oligonucleotide detection probes and introduced into a solution of the single-stranded target oligonucleotide. A polymeric network of nanoparticles is formed and a color change can be detected visually. Direct electrical detection

(Electrical detection), Figure 2, is one of the simplest methods for bioaffinity sensing (Natalia *et al.*, 2006).
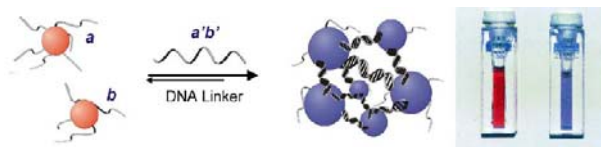
Figure 1 Properties of DNA-functionalized gold nanoparticles. A mixture of gold nanoparticles with surface-immobilized complementary DNA sequences (a, b) appears red in color and has a strong absorbance at 520 nm. When a complementary DNA sequence (a′b′) is added to the solution, the particles are reversibly aggregated causing a red shift in the surface plasmon absorbance to 574 nm, thus, appearing purple in color.

Source: Thaxton *et al.* (2006)
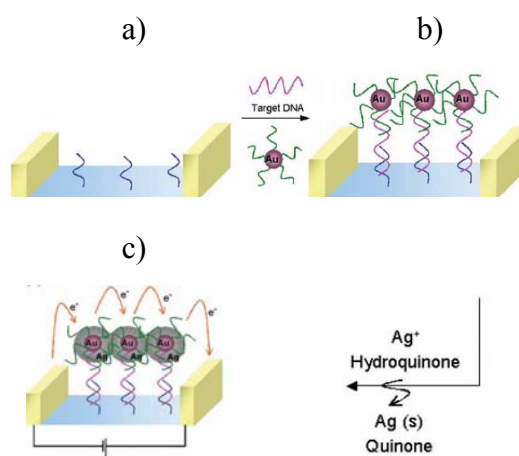
Figure 2 Electrical detection of DNA hybridization using Au nanoparticle labels. (a) Immobilization of capture probes in the gap between two electrodes. (b) Hybridization with target DNA and Au nanoparticle-labeled detection probe. (c) Reductive deposition of Ag, creating a bridge that decreases resistance.

Source: Natalia *et al.* (2006)
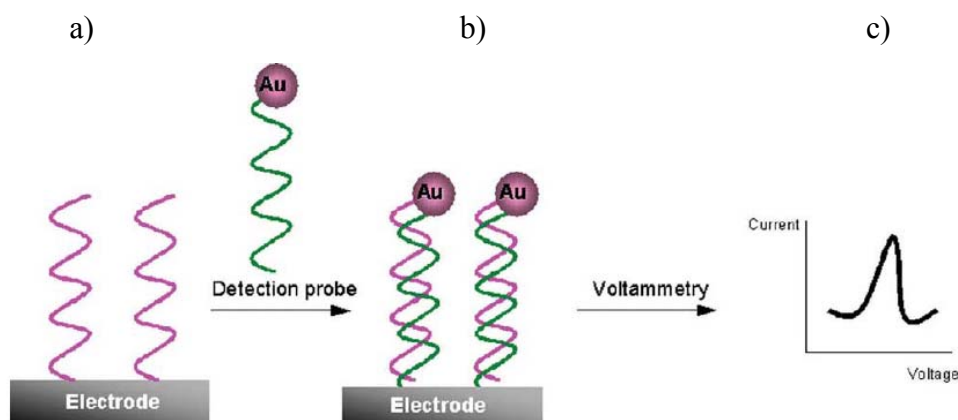
Figure 3 Electrochemical detection of DNA hybridization using Au nanoparticle labels. a) Immobilization of target DNA. b) Hybridization with Au nanoparticle labeled detection probe. c) Voltammetric detection of Au redox signal.

Source: Natalia *et al.* (2006)

The capture probes are immobilized in micron-sized gaps between electrodes in a DNA array. Hybridization with target DNA and Au nanoparticle-labeled detection probes localizes the nanoparticles in the gap, while subsequent Ag deposition creates a 'bridge' across the gap. The detection signal is the conductivity change results. The last example technique is electrochemical detection, Figure 3 (Natalia *et al.*, 2006). The redox properties of Au nanoparticles have led to their widespread use as electrochemical labels in nucleic acid detection. The target DNA imolecules are immobilized on an electrode, followed by hybridization with complementary probes labeled with Au nanoparticles. The hybrid displayed an Au oxide wave at around 1.20 V. The recent experimental and theoretical studies reported that an adenine base has the highest affinity with gold particles (Kimura-Suda *et al.*, 2003) and it preferentially binds to a nitrogen atom at the N7 position (Kryachko and Remacle, 2005b). Furthermore, there is considerable interest in applying carbon nanotubes (CNTs) that possess fascinating structural, chemical, mechanical and electrical manners as charge-transport centers for electronic transducers (Cai *et al.*, 2003; Gruner, 2006; Merkoci, 2006; Merkoci *et al.*, 2005; Valcarcel *et al.*, 2005).

These special properties of CNTs attract the interest of many researchers. One of the most important applications of CNTs in analytical chemistry is in the biosensor field. The sensor platform utilizes functionalized CNTs to detect molecular binding with high sensitivity and selectivity. It is capable of detecting a broad range of biological molecules, viz., DNA, RNA, proteins, and even cells. In DNA detection, CNTs are playing a dual role, DNA immobilization platforms and signal amplification. Some experiments are demonstrated in Figure 4. CNTs loaded with electroactive markers are shown to yield novel sensitive electrochemical detection platforms for DNA (Merkoci, 2006).
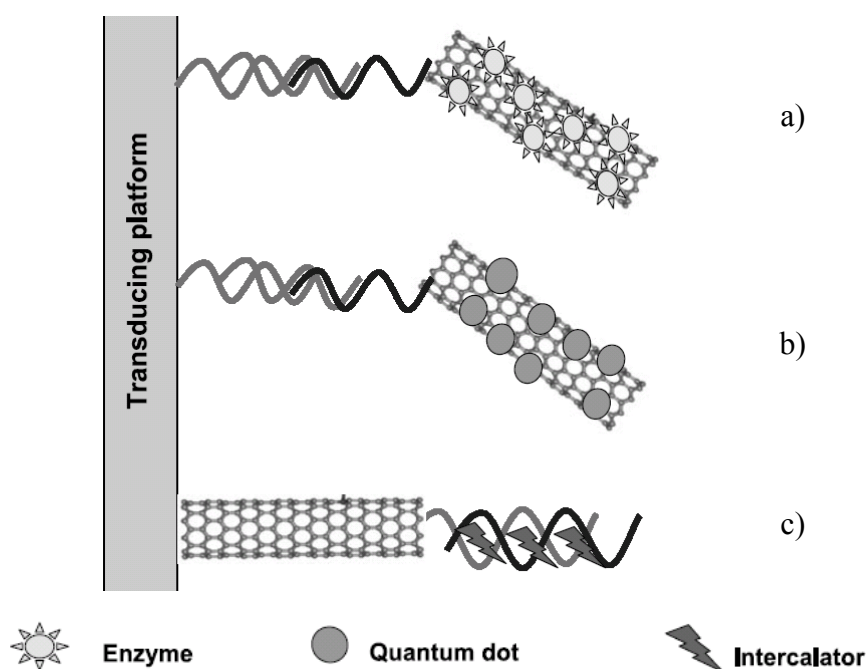
Figure 4 Schematics of various strategies used to integrate CNTs in electrochemical sensors. DNA detection via labeling with CNT loaded - a) with enzymes, b) with quantum dots and c) with intercalator.

Source: Merkoci (2006)

Hence, several experimental researches had focused on the deposition of Au NPs onto CNTs (Jiang and Gao, 2003; Liu *et al.*, 2002; Ma *et al.*, 2006; Zhang *et al.*,

2000) and there is more and more attraction to exploit a compatible assembly of them as the nanoscale building-blocks of DNA detection as depicted in Figure 5. (Lim *et al.*, 2004). They suggested that, the Au–CNT hybrid can be used as a reliable DNA hybridization biosensor. Nevertheless, there is a lack of theoretical study on the entire system, which is the combination of Au NPs, CNTs and DNA molecules.
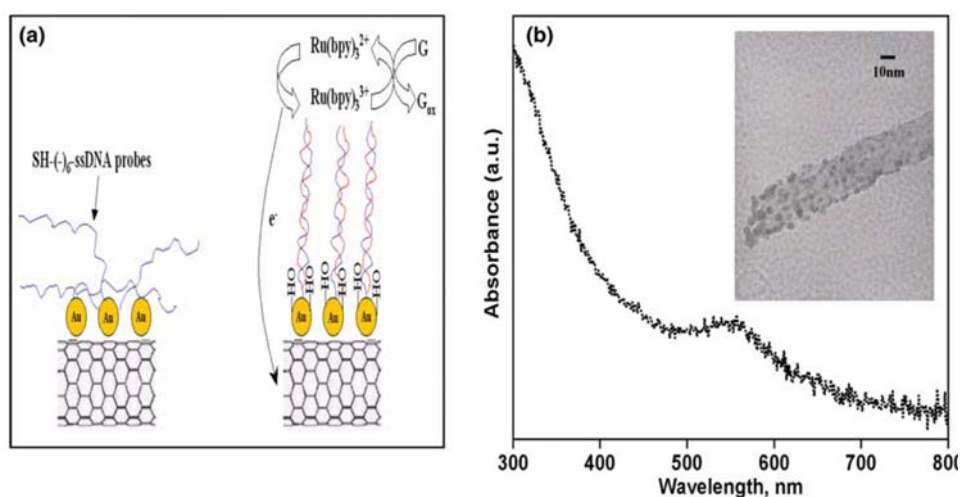
Figure 5 (a) Schematic illustration of self-assembly of thiolated oligonucleotides onto Au–CNT hybrid. The use of MCH assists the erection of ssDNA and facilitates hybridization of complementary oligonucleotides, which is detected via mediator $Ru(bpy)_3^{2+}$. (b) UV–Vis absorption spectrum of MWNT bound with gold nanoparticles. The inset shows the TEM image of a MWNT coated with gold nanoparticles.

Source: Lim *et al.* (2004)

Accordingly, it is the objective of this current work, to investigate the modulation of adenine-thymine (A:T) hybridization under the interaction with the hybrid structure of neutral gold species (Au atom and Au_3 triangular cluster) acting as the reactive sites for anchoring of the DNA bases on both types of single-walled carbon nanotubes (SWCNTs), zigzag (8,0) and armchair (5,5), to be electron transfer supports. Finally, electronic responses in the system are observed. This theoretical

study would give molecular insight to be support information for elucidation of experimental events.

LITERATURE REVIEW

DNA is a fundamental building block of life by means of the genetic code representation. In 1953, Watson and Crick discovered a famous molecular model of the double helix DNA structure (Figure 6). The double stands DNA consists of two polynucleotide chains, hold together by hydrogen bonds between complementary base pairs on opposite strands (Watson and Crick, 1953).
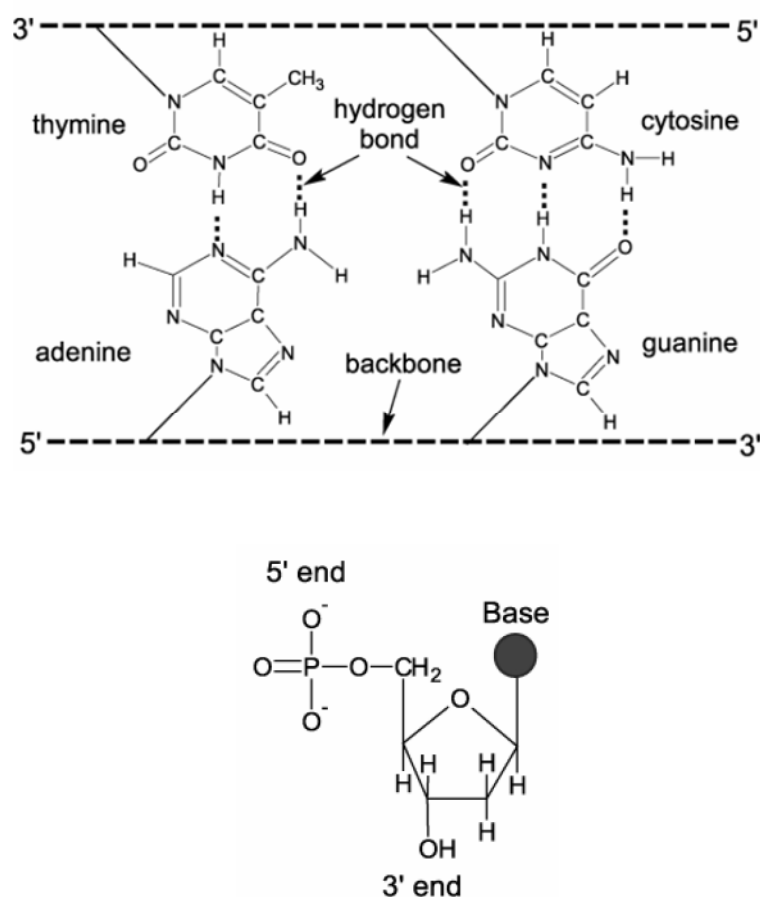
Figure 6 The four bases of DNA showing their complementary binding propertie sand DNA nucleotide.

Source: Gao and Kong (2004)

The complementary base sequences along the chain of DNA are the basis for genetic analysis and diagnosis of diseases (Vercoutere and Akeson, 2002; Zhai *et al.*, 1997). The massive amounts of genetic information have generated tremendous requiring DNA-sensors (Figure 7) with the high performance and such demands have enhanced the development of ones (Drummond *et al.*, 2003; Wang, 2002).
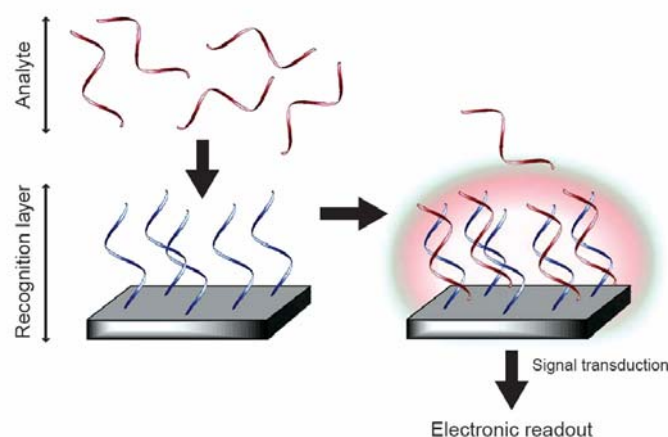
Figure 7 General DNA biosensor design. Target DNA is captured at the recognition layer, and the resulting hybridization signal is transduced into a usable electronic signal for display and analysis.

Source: Drummond *et al.* (2003)

The confluence of nanotechnology and biology, nanobiotechnology, greatly impacts on the advancement of novel biosensor design, the relation is depicted in Figure 8 (Chen *et al.*, 2004; Roco, 2003). Biology provides biomaterials and fundamental knowledge to nanotechnology, DNA is particular well suitable for biosensing applications because the hybridization with its complementary base is both specific and robust (Sun and Kiang, 2005). Nanotechnology produces the nanomaterials and nanofabrication platforms which create the miniature devices for the investigation and transformation of biological systems (Portney and Ozkan, 2006; Rogers, 2006; Vaseashta and Dimova-Malinovska, 2005). Nanostructures such as the single wall carbon nanotubes (SWCNTs), which have diameter in the 1 nm range (Figure 9), are comparable to the size of DNA molecule (the diameter of DNA

duplex). Moreover nanostructures often show new properties that are not exhibited by the bulk matter (Riu *et al.*, 2006). In recent years, there are many attempts to apply gold nanoparticles (Au NPs) and CNTs as the nanoscale building block of DNA detection devices.
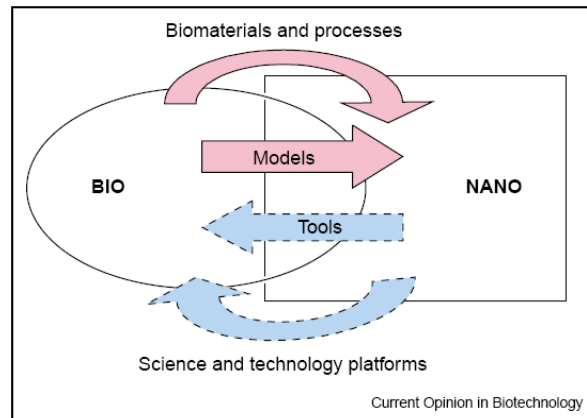
Figure 8 Key interactions between fields of biology and nanotechnology.

Source: Roco (2003)
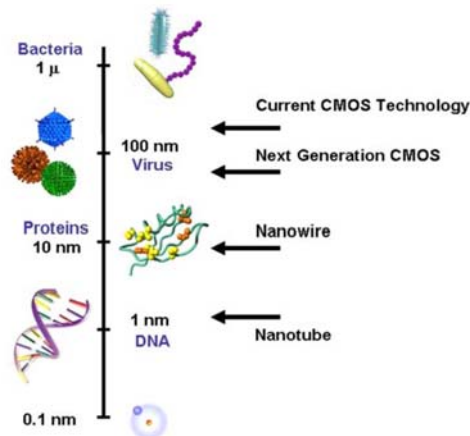
Figure 9 The dimensions of wires used in conventional CMOS technology, together with as-grown nanowires and carbon nanotubes. While the cross-section of nanofibers and inorganic nanowires is comparable to the size of typical proteins, single wall carbon nanotubes (hollow cylinders of carbon) have a diameter comparable to DNA.

Source: Gruner (2006)

The one of the most advantages of the Au NPs is enhancing the amount of immobilized biomolecules in a construction of high sensitivity DNA-sensors due to their large surface areas. They also facilitate the electron transfer across the DNA layers. In addition, it had been reported that they have very low toxicity (Daniel and Astruc, 2004; Natalia *et al.*, 2006; Shukla *et al.*, 2005; Thaxton *et al.*, 2006). Consequently, Au NPs have been used as standard supports for the anchoring of the oligonucleotides via thiol-group linkers, as shown in Figure 10 (Zhang *et al.*, 2005).
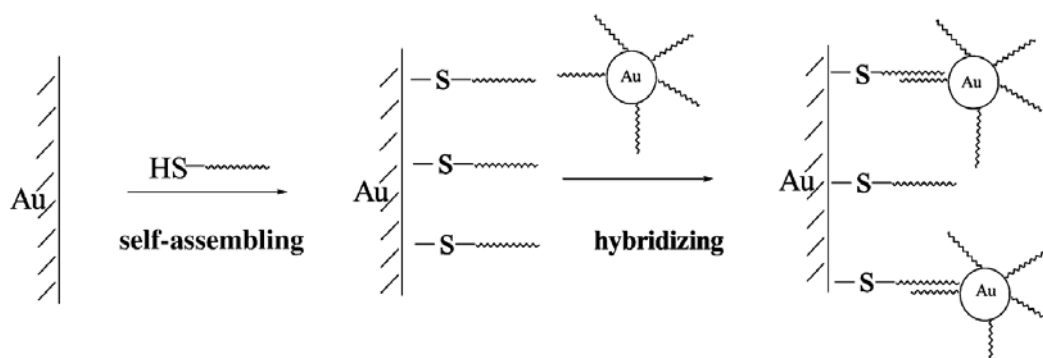
Figure 10 Schematic depiction of thiol-modified oligonucleotides self-assembling on the gold electrode and hybridizing with gold-nanoparticle-supported DNA sequences.

Source: Zhang et al. (2005)

Nowadays, CNTs (Figure 11) have attracted great attentions as nanoscale assembly for electronic devices due to their extraordinary properties including high electrical, conductivity, chemical stability and mechanical strength. Furthermore, CNTs have not only high surface-to-weight ratio (increasing the amount of DNA probe attachment) but also outstanding charge transport characteristic (promoting the electron-transfer reactions and allowing electrical communication) (Carter T. and John W., 2005; Dimitrios *et al.*, 2006; Hongjie, 2002; Merkoci, 2006). Accordingly, the utilizing of CNTs as a novel template for DNA-sensors (Figure 12) has drawn attentions from many researcher groups (Cai *et al.*, 2003; Gruner, 2006; Patolsky and Lieber, 2005; Song *et al.*, 2005; Trojanowicz, 2006; Valcarcel *et al.*, 2005).
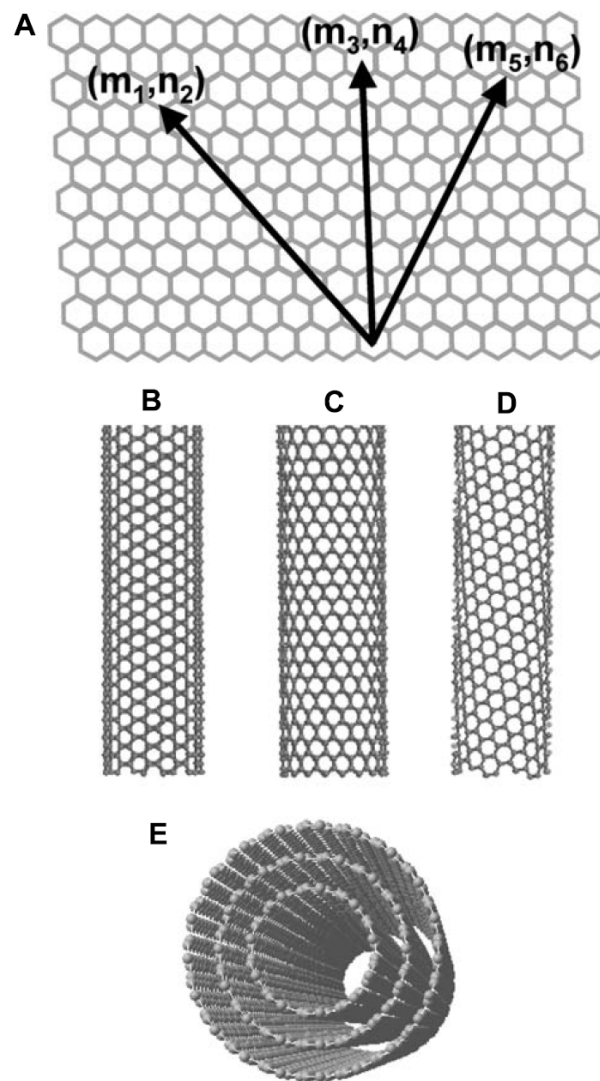
Figure 11 Schematic of the honeycomb structure of a graphene sheet (A). SWCNTs can be formed by folding the sheet along the shown lattice vectors leading to armchair (B), zigzag (C), and chiral (D) tubes, respectively. The graphene sheets rolled up into concentric cylinders form MWCNT (E).

Source: Merkoci (2006)
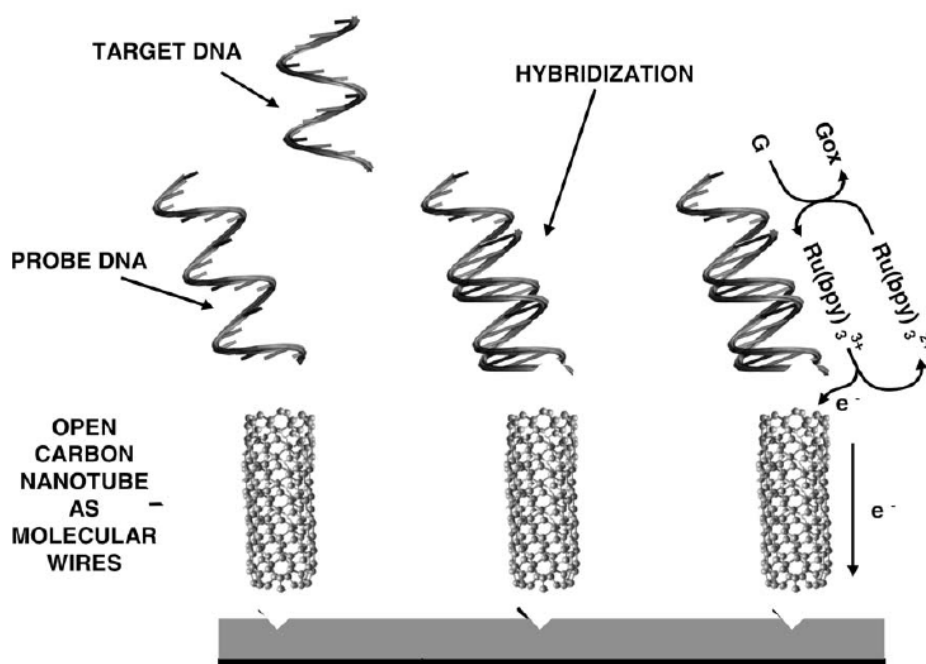
Figure 12   Schematic mechanism for nucleic acid sensing via an inlaid multi-walled carbon nanotube combined with Ru(bpy)$_3{}^{2+}$-mediator) amplified guanine oxidation.

Source: Valcarcel *et al.* (2005)

Hence, various research efforts had been made to deposit Au NPs onto CNTs (Jiang and Gao, 2003; Liu *et al.*, 2002). Xicheng Ma *et al* (Ma *et al.*, 2006) reported that Au NPs were homogeneously deposited on the surface of the CNTs by using electroless plating technique and displayed a spherical shape with a sharp particle size distribution centered at around 3–4 nm (Figure 13) and suggested that the results presented in this work probably provide new catalysts with improved performance. Moreover, San Hua Lim *et al* (Lim *et al.*, 2004) investigated Au–CNT hybrid properties for as platforms of the electrochemical genosensing. In their experiments, single stranded thiolated oligonucleotide probes were immobilized onto the Au–CNT hybrid through gold–sulfur linkage and CNTs played a complementary role as a support (Figure 5). After that they detected the catalytic oxidation current, they concluded that it could be used as a reliable DNA hybridization biosensor.
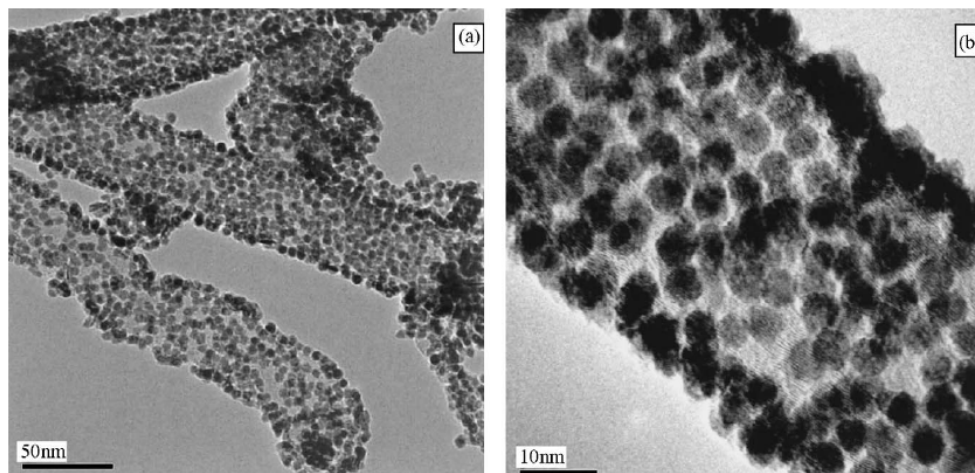
Figure 13   Representative HRTEM micrographs showing (a) low-magnification and (b) high-magnification views of Au nanopartice supported on a carbon nanotube.

Source: Ma *et al.* (2006)

However, there is a lack of theoretical study on the entire system which is the combination of Au NPs, CNTs and DNA molecules. Therefore, it is the aim of this work, to investigate the modulation of base pair hybridization (the essential principle of DNA sensors) under the interaction with hybrid structure of neutral gold species, Au atom and Au$_3$ triangular cluster, simplest stable one (Bravo-Perez et al., 1999; Kryachko and Remacle, 2005a; 2005b; Wells et al., 2004) and single walled-CNTs (sidewall reactive forms).

By the way, Kimura-Suda, H *et al* (Kimura-Suda *et al.*, 2003) reported the relative binding affinities of four nucleobases for adsorption on polycrystalline Au films obeyed the following order: adenine(A) > cytosine(C) ≥ guanine(G) > thymine(T) and Demers, L. *et al* (Demers *et al.*, 2002) also reported the heats of desorption, ΔH_{des} of the DNA bases from Au films by temperature-programmed desorption (TDP) method that equal to ΔH_{des}(T) = 26.5 ± 0.5 kcal/mol; ΔH_{des} (C) = 30.6 ± 1.0 kcal/mol; ΔH_{des} (A)) = 31.3 ± 0.7 kcal/mol; and ΔH_{des} (G) = 34.9 ± 0.5 kcal/mol. E. S. Kryachko *et al* (Kryachko and Remacle, 2005a) calculated (at the

B3LYP/RECP (gold) U 6-31++G(d,p) level) the averaged binding energies over site, adenine base possesses the highest average affinity to Au_3, 19.8 kcal/mol. The average affinity to Au_3 of cytosine, guanine and thymine were 18.9, 16.5 and 12.5 kcal/mol respectively. Thereby, the above information guides me to study the alteration of adenine-thymine base pair (adenine anchoring) because it has highest affinity with Au nanostructures. Additionally, Sigel, H. *et al* (Sigel, 1993) showed the experimental results of nucleobases-transition metal ion complexes stability, the following order of stability was valid for the transition metal ion binding sites at neutral pH: N7/O6(G) > N3(C) > N7(A) > N1(A) > N3(A,G). E. S. Kryachko *et al* (Kryachko and Remacle, 2005b) optimized geometries of DNA bases-Au_3 complexes (Figure 14) at the B3LYP/RECP (gold) U 6-31++G(d,p) level, the distances of any anchoring sites of adenine are 2.153 Å (A-Au_3(N1)), 2.138 Å (A-Au_3(N3)) and 2.243 Å (A-Au_3(N6)), 2.130 Å (A-Au_3(N7)). The shortest Au-N bond (2.130 Å) is formed in the A-Au_3(N7) complex. They also optimized geometries of DNA bases pair-Au_3 complexes (Figure 15) at the same level, 2.138 Å [A-Au_3(N3)]:T, 2.235 Å [A-Au_3(N6)]:T and 2.131 Å (A-Au_3(N7)). Such experimental and theoretical researches concluded that the adenine base preferentially binds to Au atom and Au_3 cluster at N7 position. From many experiments, CNTs were functionalized by acid treatments in order to activate their surfaces for linking Au NPs to them. Covalent functionalization of the sidewalls for the SWNTs provides stability and best accessibility, but damages the sidewalls leading to diminish the mechanical and electronic properties of the SWNTs. Due to this problem, non-covalent routing to nanotube functionalization offers the ease of synthesis and minimum disruption of the tubular structure. Then single stranded thiolated oligonucleotide probes were immobilized onto the Au–CNT hybrid via gold–sulfur linkage. However there are the debates of sulfur linkages role especially their resistance in molecular electronics, consequently, current studies are possible to avoid using thiol linkers (Kryachko and Remacle, 2005b).
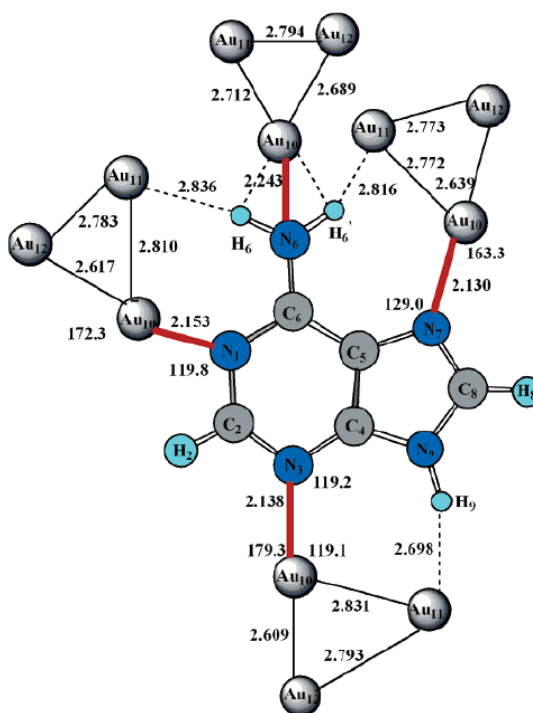
Figure 14   The four possible planar (N1, N3, N7) and nonplanar (N6) binding sites
of the gold cluster Au$_3$ to adenine. Also shown is the NH$_2$ anchored
complex A:Au$_3$ (N6). The bond lengths are given in Å and bond angles
in degrees.

Source: Kryachko and Remacle (2005a)
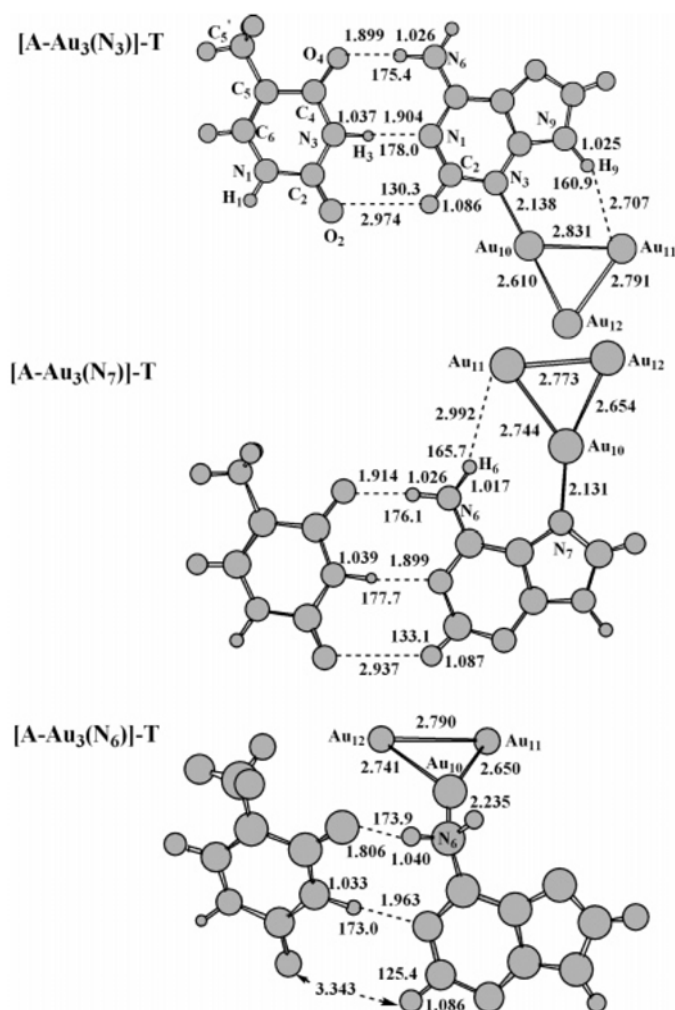
Figure 15 The stable [A-Au3]:T pairs. The WC intermolecular H-bonds of the isolated A:T pair are characterized by the following geometrical parameters: r(N6-H6(A))=1.023 Å, r(H6-O4)=1.926Å, ∠(N6H6O4)= 174.1°; r(N3-H3)=1.044Å, r(H3-N1)=1.822Å, ∠(N3H3N1)= 178.5°; r(C2-H2)=1.087Å, r(H2-O2) =2.937Å, ∠C2H2O2= 131.9°. The bond lengths are given in angstroms and bond angles in degrees.

Source: Kryachko and Remacle (2005b)

Accordingly, above overall the experimental and theoretical information is leading to construct a comprehensive model. SWCNTs play a role as a support and serve as a fast electron-transfer center, then, they interact with Au species without any linker. Au species acted as the anchoring sites directly contact with adenine molecule at N7 atom. Finally the hybridization with thymine molecule is observed.

METHODS OF CALCULATIONS

1. Perdew, Burke and Ernzerhof (PBE) Functional

The Kohn–Sham density functional theory (DFT) is the most widely-used many-body method for the electronic structure calculations of atoms, molecules, solids, and solid surfaces. The DFT theory is described in the Appendix. In this theory, only the exchange-correlation energy must be approximated as a functional of the electron density. The simplest approximation is the local spin density (LSD) approximation which uses the local electron spin densities $n_\uparrow(\mathbf{r})$ and $n_\downarrow(\mathbf{r})$ as the only ingredients. In the development of DFT, a significant step was the introduction of the density gradients $\nabla n_\uparrow(\mathbf{r})$ and $\nabla n_\downarrow(\mathbf{r})$ as additional local ingredients in the generalized gradient approximation (GGA). The Kohn–Sham kinetic energy densities are shown in Equation 1, as additional local ingredients. The reduced density gradient (Equation 2) is large in the exponential tail of the density.

$$\tau_\sigma(r) = \frac{1}{2}\sum_i |\nabla \psi_{i\sigma}(r)|^2 \qquad (\sigma=\uparrow,\downarrow) \qquad (1)$$

$$s = \frac{|\nabla n|}{2k_F n} \qquad (k_F = (3\pi^2 n)^{1/3}) \qquad (2)$$

Because of the use of the density gradients, GGA satisfies more exact constraints than LSD and as a result dramatically improves upon LSD for most chemical problems. PW91 is the first reasonable GGA that can be reliably used over a very wide range of materials. It contains much of the known correct physics of the exchange and correlation interactions. However, the most popular in materials science is nonempirical the generalized gradient approximation (GGA) of Perdew, Burke, and Ernzerhof (PBE). PBE is based on PW91 containing the correct features of LDA but ignores the correct features of PW91 that are: (1) Correct 2nd order gradient coefficients of E_x and E_c in the slowly varying limit; (2) Correct non-uniform scaling of E_x in the limits where s tends to infinity. It is known that, PBE provides a much

more realistic description of the short-range part of the van der Waals interaction than does the local spin density (LSD) approximation. Nevertheless, many density functionals have been developed in recent years in a semiempirical way and a few in a nearly or fully nonempirical way. Density functionals are said to be semiempirical if they contain parameters fitted to the experiment, and to be nonempirical if all the parameters introduced are determined only by the exact constraints imposed on them. Nonempirical density functionals can achieve usefully uniform accuracy for diverse systems, while semiempirical ones are usually highly accurate only within their training sets. This is because only the parameters fixed by exact constraints can be universal. Accordingly, the semiempirical (such as BLYP) is suitable for the chemistry approach because it is originated from the parameter fitting to produce molecular results. The nonempirical (such as PBE) is based on general arguments and is capable of describing different types of bonding. Therefore, the nonempirical is preferred for physics problems.

2. Resolution of the Identity (RI) Technique

An approximation, which efficiently reduces the computational demands without affecting significantly the accuracy, is the resolution of the identity (RI) approximation. The RI approximation leads to an enormous speed-up and so enableds us to get reliable data also for larger systems. It stands for an approximation of the computationally expensive the two-electron four-center integrals over the Gaussian basis functions by three-center integrals and proceeds by utilizing an auxiliary basis set, which is inserted as an approximated identity. Improvements in the computational efficiency of the base integral evaluation algorithms can have a significant effect on the overall speed of the calculation. This method is also available as an extension to SCF calculations and DFT.

3. Computational Methods

All the calculations were performed at the density functional theory with the Perdew, Burke and Ernzerhof (PBE) (Perdew *et al.*, 1996) non-local generalized gradient functional. Two different Dunning's correlation consistent polarized valence basis sets were employed, cc-pVDZ for SWCNTs and cc-pVTZ, for the A:T base pair moiety. For the Au atom, core electrons were represented by a relativistic corrected effective core potential (ECP), whereas 19 valence electrons were treated explicitly by (7s6p5d)/[6s3p2d] contraction. All fully relaxed optimization processes were done using the Turbomole 5.7 code (Ahlrichs *et al.*, 1989). With the intention of reducing the computational time without sacrificing accuracy, the coulomb interactions were efficiently treated by resolution of the identity (RI) technique (Eichkorn *et al.*, 1995).

On the other hand, Table 1 contains the details for expressing the reason for choosing the cc-pVTZ Dunning's basis sets in the adenine-thymine (A:T) base pair. Focusing on the major objective, the A:T base pair calculation, the B3LYP/6-31G** method on the Gaussian 03 program provides the most accurate results as compared with experimental reports. In this study, we prefer to perform calculations on the Turbomole 5.7 program due to its algorithms being more effective for big systems. Unfortunately, the Pople's style basis sets are unavailable in the Turbomole program, therefore, the quality comparison basis sets are considered. From Table 1, the cc-pVDZ basis set shows the same performance as with the 6-31G** basis set. Nevertheless, there are almost 150 atoms in our system, so we need to select the other DFT functional which is more practical. The popular BP86 and PBE GGA approximations are selected to evaluate with the cc-pVDZ basis set. We obtained poor results in both the BP86/cc-pVDZ and PBE/cc-pVDZ methods. Hence, the extension basis set, cc-pVTZ, was further investigated and we achieved better results, especially, in the PBE/cc-pVTZ method.

Table 1   Systematic evaluation of the suitable methods and basis sets for adenine-thymine base pair.

Method	Program	N1-N3 (Å)	N6-O4 (Å)	∠N1H1N3 (degree)	∠N6H6′O4 (degree)
Experiment	-	2.82	2.95	-	-
B3LYP/6-31G**	Gaussian 03	2.85	2.94	179.8	174.5
B3LYP/cc-pVDZ	Turbomole 5.7	2.85	2.94	179.8	174.4
BP86/cc-pVDZ	Turbomole 5.7	2.78	2.85	179.9	175.4
PBE/cc-pVDZ	Turbomole 5.7	2.78	2.86	179.8	175.0
BP86/cc-pVTZ	Turbomole 5.7	2.83	2.86	179.0	176.1
PBE/cc-pVTZ	Turbomole 5.7	2.82	2.88	179.6	174.7

4. Computational Models

The systematic labels on investigated configurations are illustrated in Figure 16. The semiconductor SWCNT(8,0) is comprised of 96 carbon atoms and also including hydrogen atoms at tube ends to terminate dangling orbitals. The electronic comparable model, metallic SWCNT(5,5) with 90 carbon atoms, is also chosen to make a parallel study. Along with a compromising of a computational cost, the length of SWCNT is also concerned to avoid the unreal interactions between tube-ended hydrogen atoms and the base pair. The most stable combination structure of gold species attached on each type of SWCNT is examined before taking it to construct the DNA probe. The C_S and C_{2V} symmetry operations are used for reducing the calculation time and keeping the structural arrangement of the initial input as well. However, the symmetry limitation greatly constrains some unstable geometries. Including the short tube models (insufficient area for relaxation), these structures are very difficult to optimization and they are denoted as unable to be calculated.

Our model systems are divided into four subsystems: a SWCNT, a gold atom (Au) or a gold cluster (Au_3) and the two bases (A,T). Each term of binding energy is determined as follows

$$E_b(\text{SWCNT}/\text{Au}_n/\text{A}\cdots\text{T}) \qquad = E(\text{SWCNT}/\text{Au}_n/\text{A:T}) - E(\text{SWCNT}/\text{Au}_n/\text{A}) - E(\text{T}) \qquad (3)$$

$$E_b(\text{SWCNT}/\text{Au}_n\cdots\text{A:T}) \qquad = E(\text{SWCNT}/\text{Au}_n/\text{A:T}) - E(\text{SWCNT}/\text{Au}_n) - E(\text{A:T}) \qquad (4)$$

$$E_b(\text{SWCNT}\cdots\text{Au}_n/\text{A:T}) \qquad = E(\text{SWCNT}/\text{Au}_n/\text{A:T}) - E(\text{SWCNT}) - E(\text{Au}/\text{A:T}) \qquad (5)$$

$$E_{tb}(\text{SWCNT}\cdots\text{Au}_n\cdots\text{A}\cdots\text{T}) = E(\text{SWCNT}/\text{Au}_n/\text{A:T}) - E(\text{SWCNT}) - E(\text{Au}_n)$$
$$- E(\text{A}) - E(\text{T}) \qquad (6)$$

E_b is defined as the binding energy between two subsystems in a complex separated by dot-line in the parentheses.

E_{tb} is defined as the total binding energy of all subsystems.

E is defined as the total energy of each subsystem or complexes.

n is defined as the number of Au atom (s) in each complex, for this study, n is just only 1 or 3.
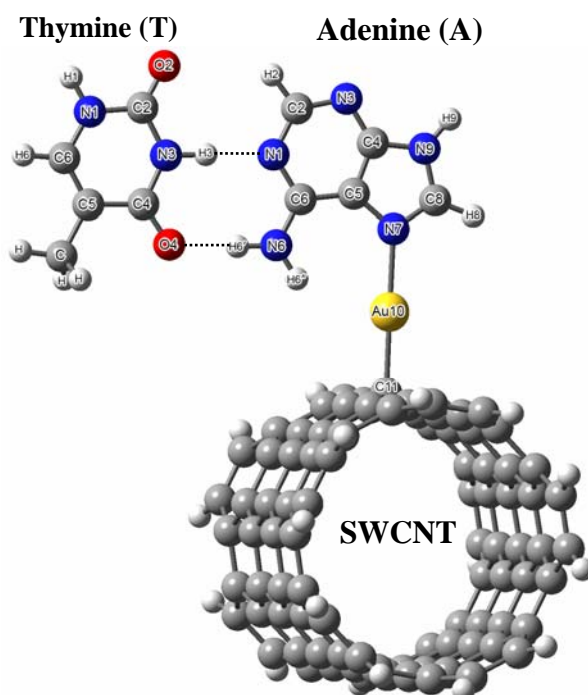
Figure 16 Illustration of studied configurations and their systematic labels of a) SWCNT/Au/A:T, b)SWCNT/Au$_3$(ApU)/A:T   and c) SWCNT/Au$_3$ (ApD)/A:T.

RESULTS AND DISCUSSIONS

1. SWCNT/gold Complexes (Hybrid Assembling Nanosupports)

The first process for DNA sensor production is a fabrication of suitable support. The CNT and gold are frontier materials for this purpose, and persuading us to study the combination properties of them. This section describes the characteristics of Au atom and Au_3 cluster deposited on both SWCNTs (SWCNT(8,0) and SWCNT(5,5)). The previous calculation, E. Durgun *et al.* (Durgun *et al.*, 2003) studied the adsorption of Au single atom on semiconducting (SWCNT(8,0)) and metallic (SWCNT(6,6)) single-wall carbon nanotubes. They reported that, the most favorable binding site of Au atom on SWCNT(8,0) was *A-T* site and on SWCNT(6,6) was *T* site (*A*; above axial C-C bond and *T*; above the carbon atom) with bond length 2.2Å and 2.3Å respectively. We also designed the behavior investigation of the Au single atom on SWCNT(8,0) and SWCNT(5,5) as their work. The overall possible deposited positions are depicted in Figure 17.
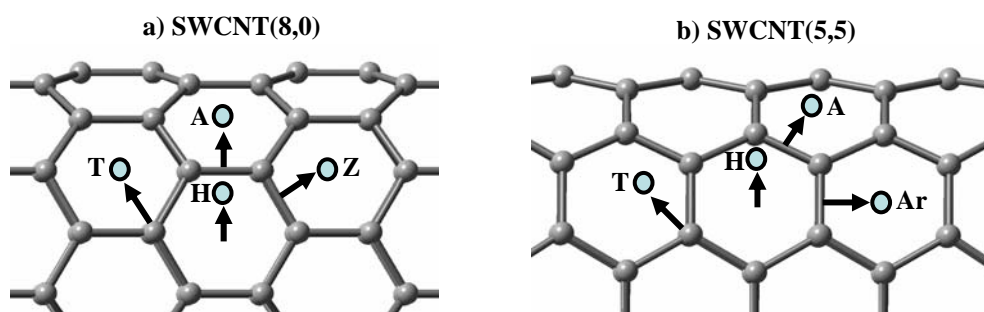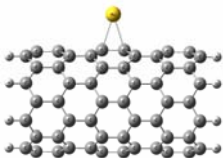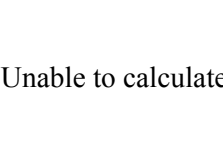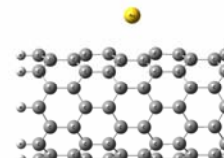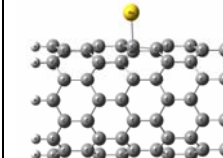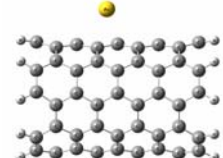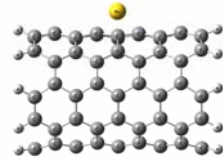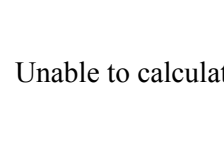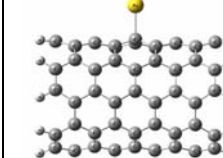
a) SWCNT(8,0)   **b) SWCNT(5,5)**

Figure 17   A schematic description of different binding sites (H, hollow; A, axial; Z, zigzag; T, top; Ar, armchair) of individual atoms adsorbed on a SWCNT(8,0) and SWCNT(5,5). Filled circles denote adatoms.

The attained results from our study also emphasize their report which as seen in Table 2 and Figure 18. Table 1 depicts all possible assemblies and their binding energies of SWCNT(8,0)/Au and SWCNT(5,5)/Au complexes which are symmetrically optimized. We found that, the top site is the most stable Au binding site on both SWCNTs (Figures 18a and 18b). Both of C_S symmetry complexes are

further calculated by fully (C_1) optimization. We display their results of the energy and the geometrical parameters in Figures 18a and 18b. The results of attached positions and Au10-C11 bond distances (2.18 Å in both complexes) from our calculation are quite resembled with E. Durgun's group. Nevertheless, the induced electronic properties of both types of SWCNTs on an attachment of Au atom are quite contrary. The SWCNT(8,0) slightly gains electrons from the Au atom while SWCNT(5,5) releases electrons to it. The magnitudes of charge transfers are just 0.005 au. in both systems (cf. Table 3). The Au atom binds with each of surfaces with binding energies of 23.1 and 21.5 kcal/mol for SWCNT(8,0)/Au and SWCNT(5,5)/Au complexes respectively.

Table 2 Symmetrical optimized geometries and calculated binding energies (E_b) of SWCNT(8,0)/Au and SWCNT(5,5)/Au complexes. The Au atom is altered deposited position on hexagonal of SWCNT (see picture) which consisting of Axial, Zigzag, Armchair; above C-C bond, Top; above the carbon atom and Hexagonal; above hollow center.

SWCNT(8,0)/Au/A:T			
Axial	**Zigzag**	**Hexagonal (Hollow)**	**Top**
C_{2V} E_b(SWCNT···Au) = 14.0 kcal/mol	C_1 (Scan the position)	C_{2v} E_b(SWCNT···Au) = 13.5 kcal/mol	C_S E_b(SWCNT···Au) = 23.5 kcal/mol
	Unable to calculate[a]		
SWCNT(5,5)/Au/A:T			
Axial	**Armchair**	**Hexagonal (Hollow)**	**Top**
C_1 (Scan the position) E_b(SWCNT···Au) = -0.8 kcal/mol	C_{2V} E_b(SWCNT···Au) = 13.2 kcal/mol	C_{2V}	C_S E_b(SWCNT···Au) = 21.6 kcal/mol
		Unable to calculate[a]	

(a) SWCNT(8,0)/Au   **(b) SWCNT(5,5)/Au**

2.18 Å   2.18 Å

$(E_b = 23.1 \text{ kcal/mol})$ $(E_b = 21.5 \text{ kcal/mol})$
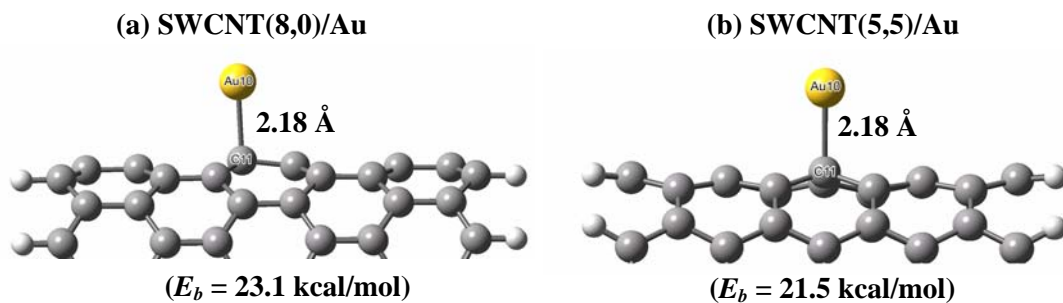
Figure 18   Fully optimized geometries, calculated binding energies (E_b) and deposited distances of the most stable structure of a) SWCNT(8,0)/Au and b) SWCNT(5,5)/Au complexes. From a) and b) demonstrate that the Au atom prefers deposition on SWCNT with top site binding.

Moreover, we also focus on finding out the stable incorporated structure of the Au_3 cluster sited on SWCNT. Among several binding characteristics, we catalog them into three major binding modes of Au_3 cluster, its basal contact (ApU), its apex contact (ApD) and its plane contact (Horizontal). Pictures and binding energies of each binding modes are demonstrated in Tables 3, 4 and 5. The abbreviations of input configurations define the directions of Au_3 cluster plane on SWCNT as follow; PDAx is perpendicular and ALAx is along to the axis of SWCNT. We also define the position of Au_3 apex atom with respected to the hexagonal of SWCNT as follows; ApH, ApB and ApT are above hollow center, above c-c bond and above carbon atom, respectively.

Table 3 Symmetrical optimized geometries and calculated binding energies (E_b) of SWCNT(8,0)/Au$_3$ and SWCNT(5,5)/Au$_3$ complexes. The basal of Au$_3$ cluster is contacted on sidewall of SWCNT and defines this binding aspect as Apex-Down mode.
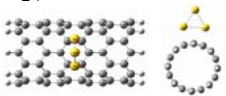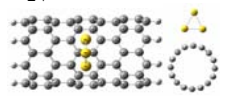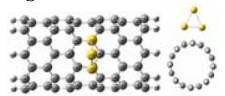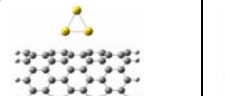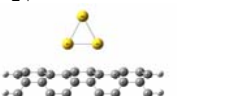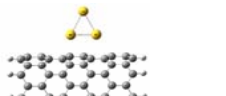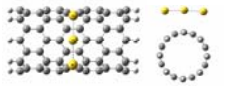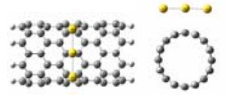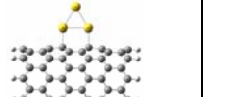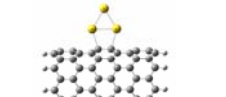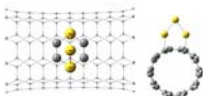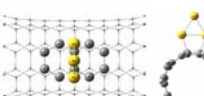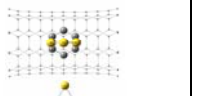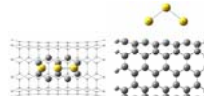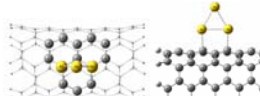
Input Configurations					
PDAx-ApH	**PDAx-ApB**	**PDAx-ApT**	**ALAx-ApH**	**ALAx-ApB**	**ALAx-ApT**
C_{2V}	C_{2V}	C_S	C_{2V}	C_{2V}	C_S
Output Configurations					
SWCNT(8,0)/Au$_3$ (ApU)					
E_b(SWCNT···Au) = 23.9 kcal/mol	E_b(SWCNT···Au) = 21.9 kcal/mol	Unable to calculate	E_b(SWCNT···Au) = 40.0 kcal/mol	E_b(SWCNT···Au) = 15.4 kcal/mol	Unable to calculate
SWCNT(5,5)/Au$_3$ (ApU)					
E_b(SWCNT···Au) = 19.8 kcal/mol	E_b(SWCNT···Au) = 25.6 kcal/mol	E_b(SWCNT···Au) = 30.0 kcal/mol	E_b(SWCNT···Au) = 14.3 kcal/mol	E_b(SWCNT···Au) = 16.9 kcal/mol	E_b(SWCNT···Au) = 22.5 kcal/mol

Table 4   Symmetrical optimized geometries and calculated binding energies (E_b) of SWCNT(8,0)/Au$_3$ and SWCNT(5,5)/Au$_3$ complexes. The apex Au atom of Au$_3$ cluster is contacted on sidewall of SWCNT and defines this binding aspect as Apex-Down mode.
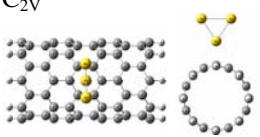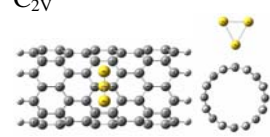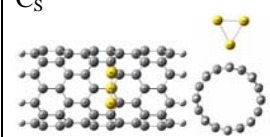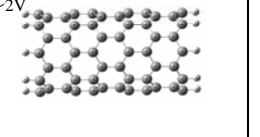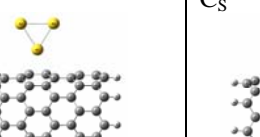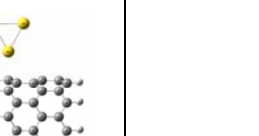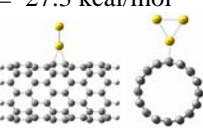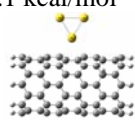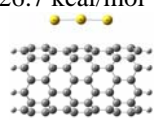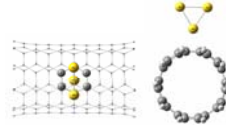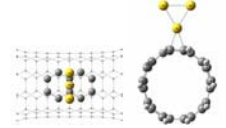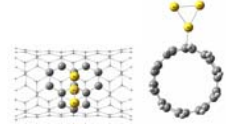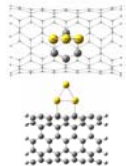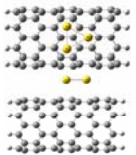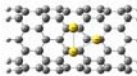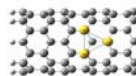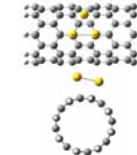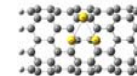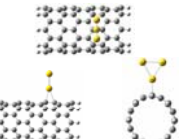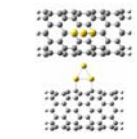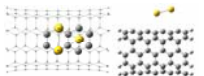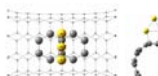
Input Configurations					
PD-ApH	**PDAx-ApB**	**PDAx-ApT**	**ALAx-ApH**	**ALAx-ApB**	**ALAx-ApT**
C$_{2V}$	C$_{2V}$	C$_S$	C$_{2V}$	C$_{2V}$	C$_S$
Output Configurations					
SWCNT(8,0)/Au$_3$ (ApD)					
E_b(SWCNT⋯Au) = 13.1 kcal/mol	E_b(SWCNT⋯Au) = 27.3 kcal/mol	Unable to calculate	E_b(SWCNT⋯Au) = 17.1 kcal/mol	E_b(SWCNT⋯Au) = 26.7 kcal/mol	Unable to calculate
SWCNT(5,5)/Au$_3$ (ApD)					
E_b(SWCNT⋯Au) = 12.6 kcal/mol	E_b(SWCNT⋯Au) = 26.9 kcal/mol	E_b(SWCNT⋯Au) = 30.0 kcal/mol	Unable to calculate	Unable to calculate	E_b(SWCNT⋯Au) = 22.6 kcal/mol

Table 5 Symmetrical optimized geometries and calculated binding energies (E_b) of SWCNT(8,0)/Au$_3$ and SWCNT(5,5)/Au$_3$ complexes. The planet of Au$_3$ cluster is contacted on sidewall of SWCNT and defines this binding aspect as Horizontal mode.

Input Configurations				
PDAx-BsH	**PDAx-BsB**	**PDAx-BsT**	**ALAx-BsT**	**ALAx-BsB**
C_S	C_S	C_S	C_S	C_S
Output Configurations				
SWCNT(8,0)/Au$_3$ (Horizontal)				
E_b(SWCNT···Au) = 28.0 kcal/mol	E_b(SWCNT···Au) = 32.0 kcal/mol	Unable to calculate	E_b(SWCNT···Au) = 40.0 kcal/mol	E_b(SWCNT···Au) = 9.3 kcal/mol
SWCNT(5,5)/Au$_3$ (Horizontal)				
PDAx-BsT	**PDAx-BsB**	**ALAx-BsH**	**ALAx-BsT**	**ALAx-BsB**
E_b(SWCNT···Au) = 12.0 kcal/mol	E_b(SWCNT···Au) = 25.6 kcal/mol	E_b(SWCNT···Au) = 22.6 kcal/mol	E_b(SWCNT···Au) = 22.6 kcal/mol	E_b(SWCNT···Au) = 22.6 kcal/mol

From Table 5, the horizontal placement of Au_3 cluster which represents the continuous Au coating on SWCNT is very unstable. Preferably, the Au_3 cluster turns its plane up to vertical direction. Therefore, the deposition of gold will have discrete particles form instead of continuous surface on SWCNT. This finding agrees with experimental work from Zhang *et al* (Zhang *et al.*, 2000)*.* The most stable structures of SWCNT(8,0)/Au_3 and SWCNT(5,5)/Au_3 complexes are illustrated in Figures 19a and 19b respectively. The Au_3 cluster interacts with the tube surface with different contact mode depending on the type of SWCNT. The Au_3 cluster in SWCNT(8,0)/Au_3 complex arranges its plane along the tube axis and attaches C14 and C13 atoms of SWCNT(8,0) by Au11 and Au12 atoms respectively. The cluster adjusts itself to be in an apex-up pattern where the Au10 atom stays on top of those by Au11 and Au12 atoms. In this rearrangement, the Au10 atom will be only a vacancy anchor point and ready to interact with the incoming base molecule. Conversely, the Au_3 cluster in SWCNT(5,5)/Au_3 complex perpendicularly contacts to the tube axis with only one atom. The Au_3 cluster arranges its apex (Au12) down to the tube surface and let its basal atoms (Au10 and Au11) point up. In this case, there are two anchor sites for the incoming molecule.

a) SWCNT(8,0)/Au$_3$ (ApU) ALAx-ApH

0.04

0.10   0.10

2.17 Å

(E_b = 40.2 kcal/mol)

b) SWCNT(5,5)/Au$_3$ (ApD) PDAx-ApT

-0.03   -0.02

0.04

2.20 Å

(E_b = 29.9 kcal/mol)
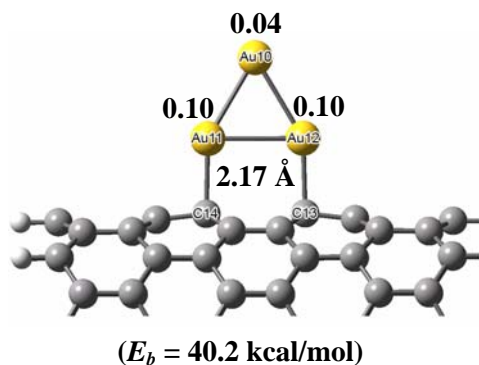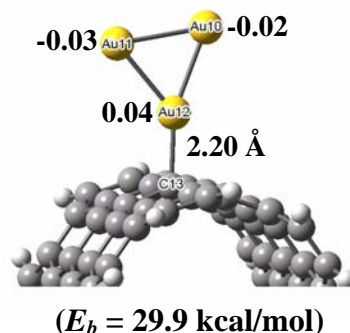
c) SWCNT(8,0)/Au$_3$ (ApU) PDAx-ApB

-0.03   -0.03

0.07

2.22 Å

(E_b = 22.5 kcal/mol)
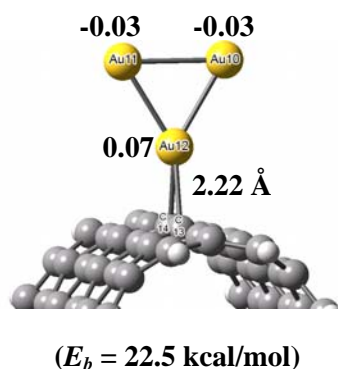
d) SWCNT(5,5)/Au$_3$ (ApD) ALAx-ApT

0.104

0.09   0.09

2.25 Å

(E_b = 27.5 kcal/mol)
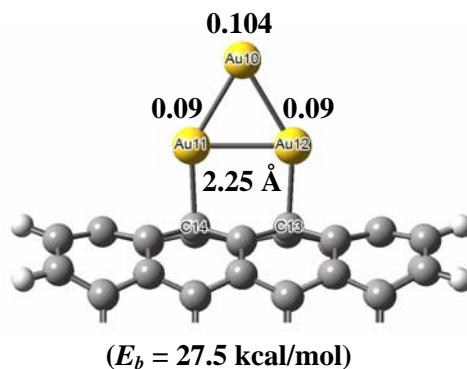
Figure 19   C$_S$ (symmetry applied) optimized geometries, calculated binding energies (E_b), deposited distances and Mulliken population charges of a) the most stable structure of SWCNT(8,0)/Au$_3$ b) the most stable structure of SWCNT(5,5)/Au$_3$ c) the most stable structure of SWCNT(8,0)/Au$_3$ that holding the Au$_3$ cluster with PD-ApD binding mode and d) the most stable structure of SWCNT(5,5)/Au$_3$ that holding the Au$_3$ cluster with AL-ApU binding mode.

From Mulliken population analysis, similar findings as in the SWCNT/Au systems are found in the SWCNT/Au$_3$ complexes. SWCNT(8,0) acts as an electron acceptor (negative charges in SWCNT(8,0)) while SWCNT(5,5) acts as an electron donor (positive charges in SWCNT(5,5)). However, we expect that the binding characteristic of the Au$_3$ cluster also influences the electron transferring phenomenon

in the SWCNT/Au$_3$ complex. Therefore, it is important to understand the electron redistribution by considering another binding mode of each SWCNT/Au$_3$ complex as shown in Figures 19c and 19d, even though both are not the next stable complexes. We observe the electron population moving from Au$_3$ cluster apex to its basal for all four complexes with not respect to the type of SWCNT. The basal Au atoms (Au11 and Au12) of Au$_3$ cluster in SWCNT(8,0)/Au$_3$(ApU) and SWCNT(5,5)/Au$_3$(ApU) continuously release electron to SWCNT, which can be asserted by the positive charges of all Au atoms. On the other hand, the electron density in SWCNT(5,5) of the SWCNT(5,5)/Au$_3$(ApD) complex is drawn to accumulate at the basal of adsorbed Au$_3$ cluster. Even though, the electrons of Au$_3$ cluster in SWCNT(8,0)/Au$_3$(ApD) are attracted to SWCNT(8,0) but somewhat electrons are still distributed to the basal Au atoms. For the binding energy point of view, the ApU binding mode structure of SWCNT(8,0)/Au$_3$(ApU) is much more stable than of SWCNT(5,5)/Au$_3$(ApU), 40.2 and 27.5 kcal/mol, respectively. The distinct energy is probably originated from, not only the SWCNT-Au$_3$ intermolecular distance in SWCNT(8,0)/Au$_3$(ApD) complex is shorter but also the C13-C14 bond length in SWCNT(8,0) tube (~2.87 Å) is more fitting with incoming Au$_3$ cluster (Au-Au bond length ~ 2.80 Å) than in SWCNT(5,5) tube (~2.52 Å). We complete our work by employing the whole of SWCNT/Au$_3$ complexes as shown in Figure 19 to interact with adenine base despite the fact that the SWCNT(8,0)/Au$_3$(ApD) and SWCNT(5,5)/Au$_3$(ApU) complexes are not the best stable complex of each kind of SWCNT. Turning to the binding energy between Au$_3$ cluster and SWCNT, it is rather associated with contact distance. There is the shortest Au$_3$-SWCNT bond length (2.17 Å) in SWCNT(8,0)/A$_{u3}$(ApU), as such it is the most stable SWCNT/Au$_3$ complex (40.2 kcal/mol). Its interaction energy is also quite greater than one of SWCNT(8,0)/Au$_3$(ApD) about 12.7 kcal/mol. While the intermolecular adsorption in SWCNT(5,5)/Au$_3$(ApU) complex is weaker than SWCNT(5,5)/Au$_3$(ApD) with only just magnitude of 7.4 kcal/mol. These outcomes convince us to assume that, the both binding characteristics (ApU and ApD) of Au$_3$ cluster may be occurred in SWCNT(5,5)/Au$_3$ system but there are a few possibilities to form ApD binding mode in the SWCNT(8,0)/Au$_3$ system.

2. SWCNT/Gold/Adenine Complexes (DNA Sensor Probe)

The appropriate transducer is able to improve DNA sensor efficiency for the adsorption of single stranded nucleic acid and the amplification of double stranded hybridization signal. The incorporation capability of nanostructure-based transducer with probe molecule is the important topic for biosensor development. The immobilization of adenine base on hybrid supporter is observed and described in this section. Furthermore, the extra exploitation of SWCNT/gold beyond as the platform for DNA probe construction is as the sensing material for nucleic acid (target adenine molecule). We also concentrate on this issue. The optimized geometries are depicted in Figures 21, 22 and 23 and investigated parameters (intermolecular bond length, binding energy and molecular Mulliken charges) are tabulated in Tables 6, 7, and 8 for all complexes in this study. We also take account of Au/A, Au/A:T, Au_3/A and Au_3/A:T complexes as references (Figure 20). The novel combinative SWCNT/gold materials are compared to familiar bare gold species to validate a performance of the candidature support.

34
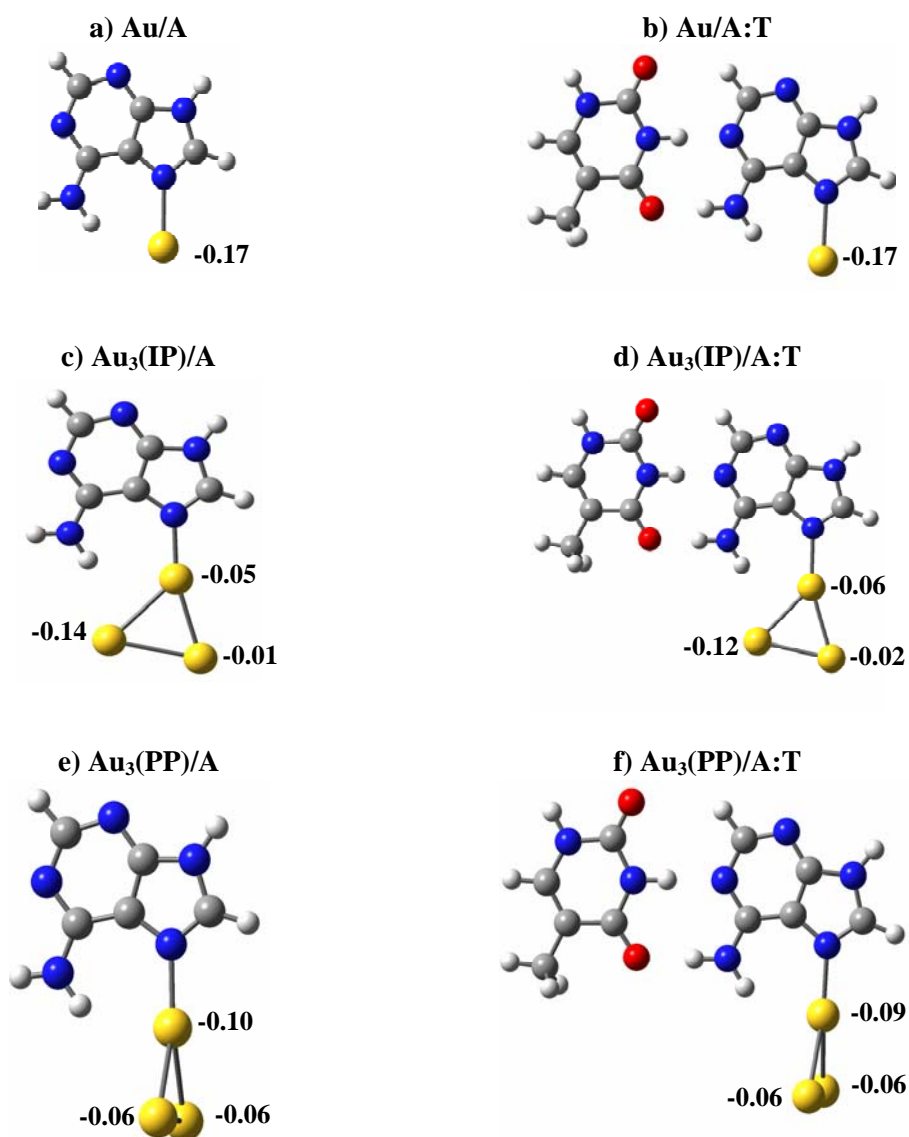
Figure 20 Fully optimized geometries[a] and Mulliken population atomic charges of the a) Au/A and b) Au/A:T. C_S (symmetry applied) optimized geometries and Mulliken population atomic charges of c) $Au_3(IP=inplane)/A$, d) $Au_3(IP)/A:T$, e) $Au_3(PP=perpendicular\ plane)/A$ and f) $Au_3(PP)/A:T$.

[a] There are two configurations of $Au_3/A:T$ structures which are investigated in this study; the Au_3 cluster is the perpendicular plane (PP) or in plane (IP) alignment respect to the A:T molecular plane.
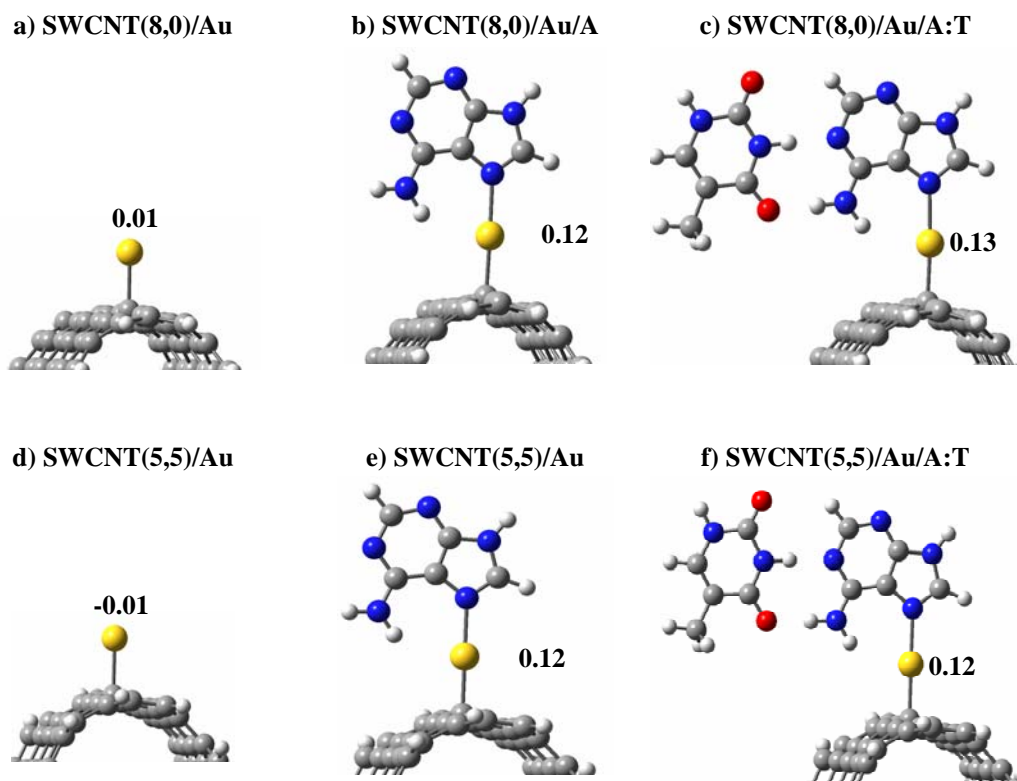
Figure 21 C$_S$ (symmetry applied) optimized geometries and Mulliken population
atomic charges of the a) SWCNT(8,0)/Au b) SWCNT(8,0)/Au/A c)
SWCNT(8,0)/Au/A:T d) SWCNT(5,5)/Au e) SWCNT(5,5)/Au f)
SWCNT(5,5)/Au/A:T. The SWCNT/A:T system are constructed from the
most stable of each SWCNT/Au complex (see Figure 19).

a) SWCNT(8,0)/Au₃(ApD)
PDAx-ApB

b) SWCNT(8,0)/Au₃(ApD)/A

c) SWCNT(8,0)/Au₃(ApD)/A:T

d) SWCNT(5,5)/Au₃(ApD)
PDAx-ApT

e) SWCNT(5,5)/Au₃(ApD)/A
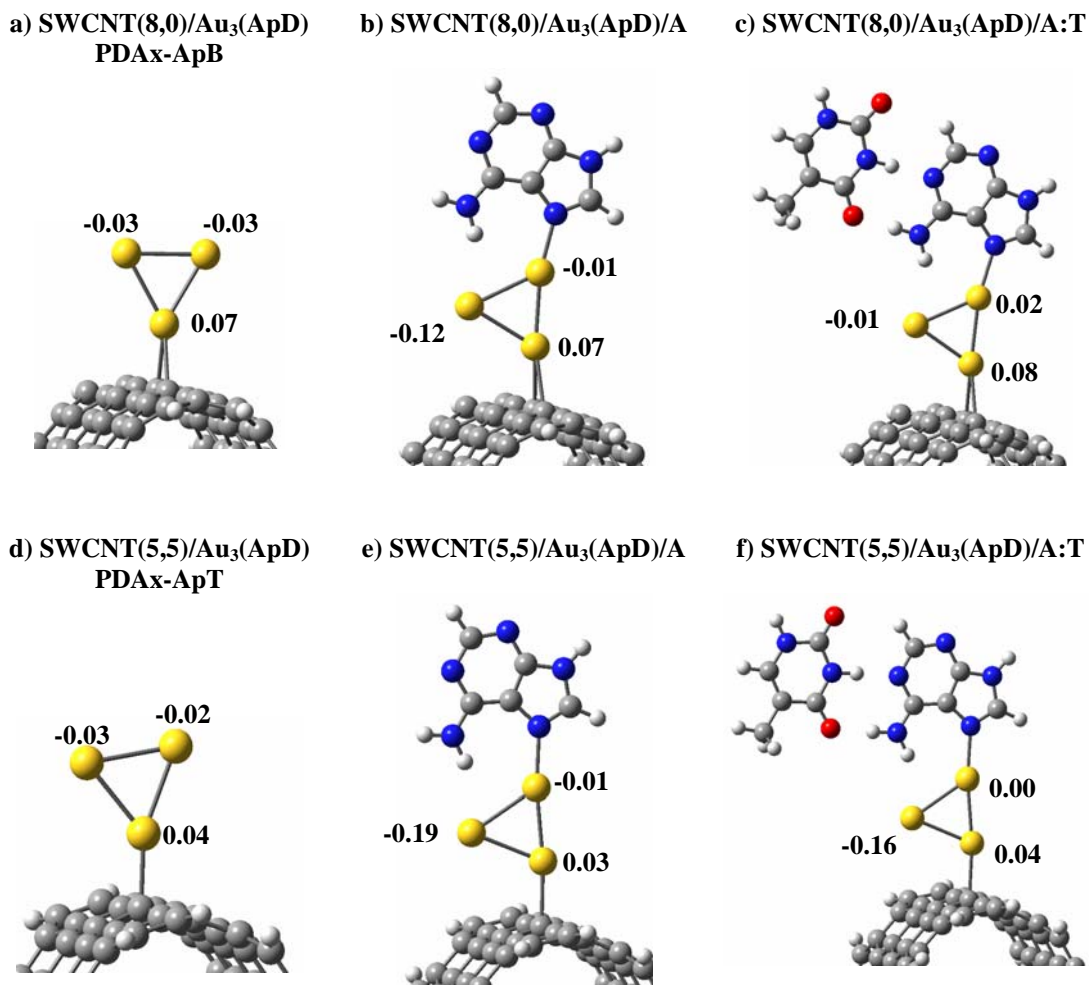
f) SWCNT(5,5)/Au₃(ApD)/A:T

Figure 22 C_S (symmetry applied) optimized geometries and Mulliken population atomic charges of the a) SWCNT(8,0)/Au₃(ApD) that hold the Au₃ cluster with PDAx-ApB binding mode b) SWCNT(8,0)/Au₃(ApD)/A c) SWCNT(8,0)/Au₃(ApD)/A:T d) the most stable structure of SWCNT(5,5)/Au₃(ApD) that hold the Au₃ cluster with PDAx-ApT binding mode e) SWCNT(5,5)/ Au₃(ApD)/A f) SWCNT(5,5)/ Au₃(ApD)/A:T. The b and c complexes are constructed from a complex and e and f complexes are constructed from d complex.

a) SWCNT(8,0)/Au₃(ApU)
ALAx-ApH

b) SWCNT(8,0)/Au₃(ApU)/A

c) SWCNT(8,0)/Au₃(ApU)/A:T

d) SWCNT(5,5)/Au₃(ApU)
ALAx-ApT

e) SWCNT(5,5)/Au₃(ApU)/A
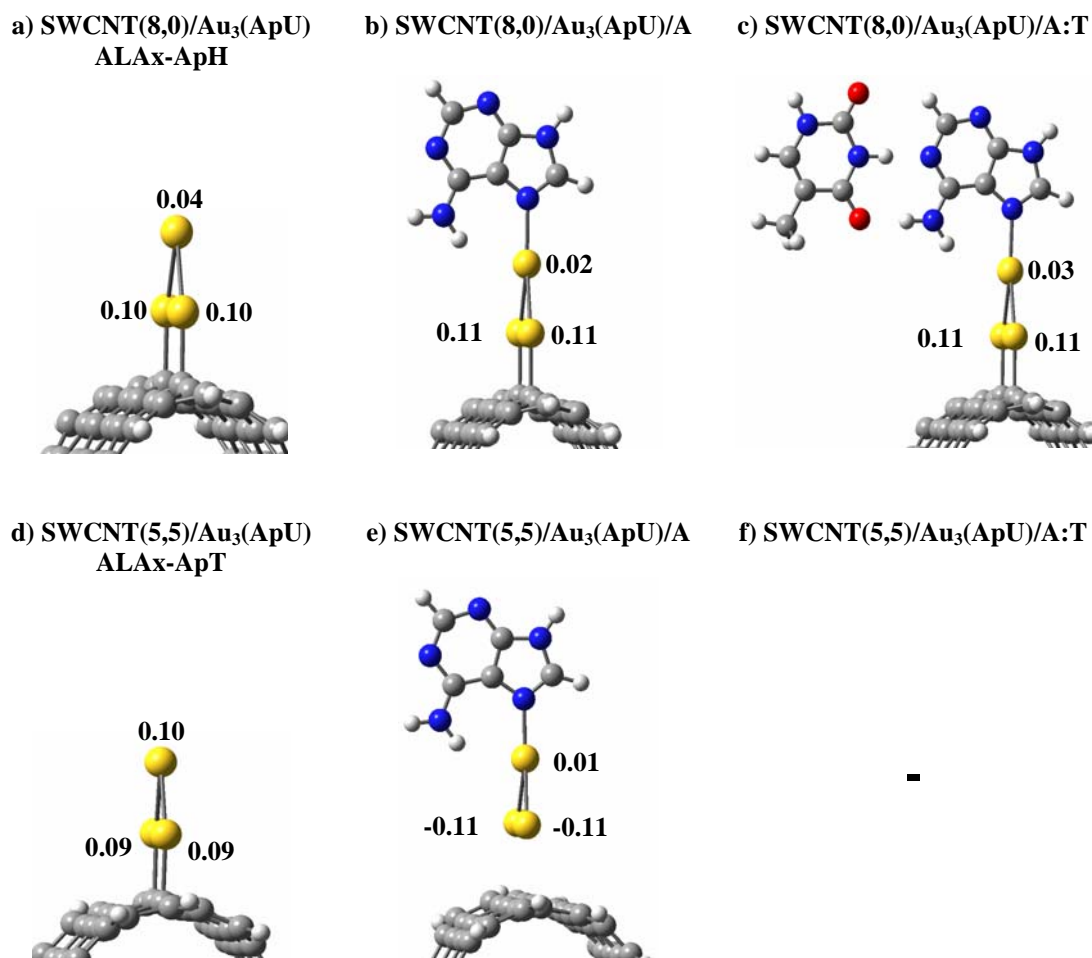
f) SWCNT(5,5)/Au₃(ApU)/A:T

Figure 23 C_S (symmetry applied) optimized geometries and Mulliken population atomic charges of a) the most stable structure of SWCNT(8,0)/Au₃(ApU) that hold the Au₃ cluster with ALAx-ApH binding mode b) SWCNT(8,0)/Au₃(ApU)/A c) SWCNT(8,0) /Au₃(ApU)/A:T d) SWCNT(5,5)/Au₃(ApU) that hold the Au₃ cluster with ALAx-ApT binding mode e) SWCNT(5,5)/Au₃(ApU)/A. The b and c complexes are constructed from a complex and e complex is constructed from d complex. The e complex is unstable so the f) SWCNT(5,5)/Au₃(ApU)/A:T complex is ignored.

Table 6 The geometrical parameters, calculated binding energies (E_b), energy gap and Mulliken population molecular charges of the Au/A:T, SWCNT(8,0)/ Au/A:T, SWCNT(5,5)/Au/A:T and their fragments.

	Au/A	Au/A:T	SWCNT/ Au	SWCNT/ Au/A	SWCNT/ Au/A:T
Distance & Energy					
r (N7-Au10) Å, (E_b(SWCNT/Au···A:T)) kcal/mol					
SWCNT(8,0) Complexes			-	2.14 (19.2)	2.14 (18.3)
SWCNT(5,5) Complexes	2.26 (14.1)	2.26 (13.4)	-	2.14 (22.4)	2.14 (22.0)
r (Au10-C11) Å, (E_b(SWCNT···Au/A:T)) kcal/mol					
SWCNT(8,0) Complexes			2.18 (23.1)	2.11 (28.2)	2.12 (28.0)
SWCNT(5,5) Complexes	-	-	2.18 (21.5)	2.12 (29.9)	2.12 (30.1)
E_{tb}(SWCNT···Au···A···T) kcal/mol					
SWCNT(8,0) Complexes	14.05	29.83	23.1	42.3	57.8
SWCNT(5,5) Complexes			21.5	44.0	60.0
Energy Gap (eV)					
SWCNT(8,0) Complexes	0.85	0.85	0.30	0.27	0.27
SWCNT(5,5) Complexes	(0.72)[a]		0.13	0.13	0.13
Charge (au.)					
q_M(A) & q_M(T)					
SWCNT(8,0) Complexes		0.204 & -0.032	-	0.276	0.291 & - 0.010
SWCNT(5,5) Complexes	0.170	(0.046 & -0.046)[b]	-	0.271	0.295 & - 0.017
q_M (Au)					
SWCNT(8,0) Complexes			0.005	0.123	0.128
SWCNT(5,5) Complexes	- 0.170	- 0.172	-0.005	0.122	0.122
q_M (SWCNT)					
SWCNT(8,0) Complexes			-0.005	-0.399	-0.408
SWCNT(5,5) Complexes	-	-	0.005	-0393	-0.401

[a] The energy gap of the original A:T base pair

[b] Mulliken charge of adenine and thymine molecules in A:T base pair.

2.1 DNA Probe Stability

From Table 6, it should undoubtedly be observed that the most sensitive geometrical parameters due to an assembling of the base pair, gold atom and SWCNT are Au10-N7 and Au10-C11 bonds. The Au10-N7 bonds are obviously contracted from 2.26 Å in Au/A to 2.14 Å in both SWCNT(8,0)/Au/A and SWCNT(5,5)/Au/A complexes. Similar results are found for the Au10-C11 bond, the interactions of A or A:T cause the Au10-C11 bond to shorten from 2.18 Å to around 2.12 Å in both SWCNT(8,0)/Au and SWCNT(5,5)/Au systems. These findings refer to an effectiveness of the integration between SWCNTs and gold particles for being a steady probe because it enhances an immobilization of the recognition layer via a cooperative effect of SWCNTs, gold particles and DNA base compartments. Considering of the energetic results, it should be noted that both types of SWCNTs improve the strength of the interaction between the gold atom and the adenine base. In comparison to the Au/A complex, the binding energies between the gold atom and the base pair are increased by 5.1 kcal/mol in the SWCNT(8,0)/Au/A complex and by 8.3 kcal/mol in the SWCNT(5,5)/Au/A complex. Likewise, the interaction between the gold atom and the SWCNT is increased after interacting with the adenine base. The magnitude of E_b(SWCNT$\cdots$Au/A:T) is increased by 5.1 and 8.4 kcal/mol as in SWCNT(8,0)/Au/A and SWCNT(5,5)/Au/A complexes, respectively, when compared with the SWCNT/Au system. Overall, for binding energy analysis, it could be mentioned that the energy characteristics of SWCNT(8,0)/Au/A complexes quite resemble the SWCNT(5,5)/Au/A complex. This events guide us to conclude that SWCNT/Au hybrid structures are effective nanomaterials for adenine immobilization and adenine itself acts as a post treatment for SWCNT/Au ones. The Mulliken population analysis is also shown in Figure21 and Table 6. The interaction of Au and SWCNT with the adenine base causes the electron loss in the adenine molecule (more positive charge). This phenomenon can be explained by intrinsic electron withdrawing properties of the gold atom as well as outstanding charge transport characteristics of SWCNTs. These manners are emphasized by negative charges of the gold atom and SWCNT after binding with the adenine base. Especially for the Au atom, it not only performs as a good linker but also enhances the electron transfer

from the adenine base to SWCNT, which leads to an electron loss on Au and Adenine by 0.12 au. and 0.27 au., respectively, and an electron gaining on SWCNT by -0.39 au. in both types of the SWCNTs/Au/A complexes.

Table 7 The geometrical parameters, calculated binding energies (E_b), energy gap and Mulliken population molecular charges of the Au_3(IP)/A:T[a], SWCNT(8,0)/Au_3(ApD)/A:T, SWCNT(5,5)/Au_3(ApD)/A:T and their fragments.

	Au_3(IP)/A	Au_3(IP)/A:T	SWCNT/Au_3(ApD)	SWCNT/Au_3(ApD)/A	SWCNT/Au_3(ApD)/A:T
Distance & Energy					
r (N7-Au10) Å, (E_b(SWCNT/Au···A:T)) kcal/mol					
SWCNT(8,0) Complexes			-	2.15 (23.2)	2.15 (22.0)
SWCNT(5,5) Complexes	2.10 (35.5)	2.10 (34.4)	-	2.16 (19.4)	2.17 (17.8)
r(Au12-C13) or r(Au12-SWCNT) Å, (E_b(SWCNT···Au/A:T)) kcal/mol					
SWCNT(8,0) Complexes			2.22 (27.5)	2.30 (15.2)	2.30 (15.1)
SWCNT(5,5) Complexes	-	-	2.20 (29.9)	2.34 (13.7)	2.34 (13.3)
E_{tb}(SWCNT···Au···A···T) kcal/mol					
SWCNT(8,0) Complexes	35.5	50.8	27.5	50.7	65.9
SWCNT(5,5) Complexes			29.9	49.3	64.0
Energy Gap (eV)					
SWCNT(8,0) Complexes	0.50	0.50	0.10	0.18	0.17
SWCNT(5,5) Complexes	(0.03)[c]		0.18	0.02	0.03
Charge (au.)					
q_M(A) & q_M(T)					
SWCNT(8,0) Complexes	0.198	0.220 & -0.017	-	0.188	0.211 & -0.020
SWCNT(5,5) Complexes		(0.046 & -0.046)[b]	-	0.171	0.203 & -0.026
q_M (Au$_3$)					
SWCNT(8,0) Complexes	-0.198	-0.203	0.019	-0.034	0.000
SWCNT(5,5) Complexes			-0.012	-0.165	-0.118
q_M (SWCNT)					
SWCNT(8,0) Complexes	-	-	-0.019	-0.153	-0.191
SWCNT(5,5) Complexes			0.012	-0.006	-0.059

[a] The energy gap of the original A:T base pair

[b] Mulliken charge of adenine and thymine molecules in A:T base pair.

There are two adsorbed characters of Au_3 cluster, defined as in plane (IP) and perpendicular plane (PP). Au_3/A and Au_3/A:T complexes would be studied as well. The entire calculated geometries and parameters of them are contained in Tables 7 and 8. The Au_3(IP) system is slightly stable than Au_3(PP) one around 0.6-1.1 kcal/mol even if it possesses the equal anchor bond length and lesser intermolecular transferred charge. This reason involves with the existing of further interaction at exocyclic $N6^{..}H6$" of adenine base and Au11 of Au_3 cluster in Au_3(IP) system but be occurred in Au_3(PP) one. Optimized geometries, geometrical parameters, calculated binding energies (E_b), energy gap and Mulliken population molecular charges in the Au_3(IP)/A:T, SWCNT/Au_3(ApD)/A:T complexes and their fragments are shown in Figures 20, 22 and Table7. The Au10-N7 bonds length of both SWCNT(8,0)/ Au_3(ApD)/A and SWCNT(5,5)/ Au_3(ApD)/A are longer by 0.05Å as compared with Au_3(IP)/A. Moreover, Au12-C13 bonds of both SWCNT/Au_3(ApD) are lengthen by 0.08-0.14Å after interacted with adenine. The reducing of binding energies of two bonds (Au10-N7 and Au12-C13) attributes to the elongation of their bond lengths (cf. in Table 7). Regarding to Mulliken charges, the electrons in adenine bases are drawn to both SWCNTs/Au_3(ApD) in spite of Au10 active sites are bearing the negative charges. Owing to negative charges, the amount of transferred charges from adenine to SWCNTs/Au_3(ApD) is less than to bare Au_3 cluster. Surprisingly, the whole of prior observations indicate that, all of electrons from adenine base is continuously transferred to SWCNT but in the case of SWCNT(8,0)/Au_3(ApD)/A and SWCNT(5,5)/Au_3(ApD)/A, there are electron accumulation on vacancy site Au11 atom. This event is emphasized by the more negative charges on Au11 atom from -0.03 au. in both of SWCNT(8,0)/Au_3(ApD) and SWCNT(5,5)/Au_3(ApD) to -0.12 au. and -0.19 au. in SWCNT(8,0)/Au_3(ApD)/A and SWCNT(5,5)/Au_3(ApD)/A, respectively. The Au11 atom performing as electron donor can interact with electron acceptor, N6-H6" of adenine molecule, to form as nonconventional hydrogen bond. The nonconventional hydrogen bond distances (r(N6-Au)) are detailed in Table 9. These bonds in both SWCNT(8,0)/Au_3(ApD)/A and SWCNT(5,5)/Au_3(ApD)/A complexes are shorter than in Au_3(IP)/A complex by 0.08 and 0.14 Å. This interaction might be a reason of the Au12-C13 stretching.

Table 8 The geometrical parameters, calculated binding energies (E_b), energy gap and Mulliken population molecular charges of the $Au_3(IP)/A{:}T$, $Au_3(PP)/A{:}T$, $SWCNT(8,0)/Au_3(ApU)/A{:}T$, $SWCNT(5,5)/Au_3(ApU)/A{:}T$ and their fragments.

	$Au_3(PP)/$ A	$Au_3(PP)/$ A:T	SWCNT/ $Au_3(ApU)$	SWCNT/ $Au_3(ApU)/$ A	SWCNT/ $Au_3(ApU)/$ A:T
Distance & Energy					
r (N7-Au10) Å, (E_b(SWCNT/Au···A:T)) kcal/mol					
SWCNT(8,0) Complexes			-	2.27 (12.1)	2.27 (11.4)
SWCNT(5,5) Complexes	2.10 (34.1)	2.10 (33.5)	-	2.12 (20.6)	-
r (Au11-C14 = Au12-C13) Å, (E_b(SWCNT···Au/A:T)) kcal/mol					
SWCNT(8,0) Complexes			2.17 (40.2)	2.21 (18.2)	2.21 (18.0)
SWCNT(5,5) Complexes	-	-	2.25 (22.5)	2.89 (9.0)	-
E_{tb}(SWCNT···Au···A···T) kcal/mol					
SWCNT(8,0) Complexes			40.2	52.2	68.0
SWCNT(5,5) Complexes	34.1	49.9	22.5	43.1	-
Energy Gap (eV)					
SWCNT(8,0) Complexes			0.02	0.09	0.06
SWCNT(5,5) Complexes	0.50 (0.03)[c]	0.50	-	-	-
Charge (au.)					
q_M(A) & q_M(T)					
SWCNT(8,0) Complexes		0.233 & -0.013	-	0.197	0.227 & -0.025
SWCNT(5,5) Complexes	0.220	(0.046 & -0.046)[b]	-	0.192	-
q_M (Au$_3$)					
SWCNT(8,0) Complexes			0.238	0.243	0.260
SWCNT(5,5) Complexes	-0.220	-0.220	0.283	-0.209	-
q_M (SWCNT)					
SWCNT(8,0) Complexes			-0.238	-0.440	-0.461
SWCNT(5,5) Complexes	-	-	-0.283	0.0165	-

[a] The energy gap of the original A:T base pair

[b] Mulliken charge of adenine and thymine molecules in A:T base pair.

From Table 8, the $Au_3(PP)$ system is taken to compare with SWCNT/ $Au_3(ApU)$ complex due to they hold the same arrangement of Au_3 cluster as respect to the plane of A:T base pair. The Au10-N7 bonds are manifestly stretched from 2.10 Å in both Au_3/A to 2.27 Å and 2.12 Å in SWCNT(8,0)/$Au_3(ApU)$/A and SWCNT(5,5)/ $Au_3(ApU)$/A, respectively. The Au11-C14 and Au12-C13 bonds are also stretched from 2.17 Å in SWCNT(8,0)/$Au_3(ApU)$ to 2.21 Å in SWCNT(8,0)/$Au_3(ApU)$/A and from 2.25 Å in SWCNT(5,5)/$Au_3(ApU)$ to 2.89 Å in SWCNT(5,5)/$Au_3(ApU)$/A. Subsequently, the binding energies of above mentioned bonds are decreased along with distances increasing (c.f. in Table 8). From the results, it can be expressed that the Au_3 cluster which attached on both SWCNTs can adsorb the adenine base not so good as bare Au_3 cluster can. Furthermore, the assembling complexes of SWCNTs/Au_3 are destabilized after interacting with an adenine base. Moreover, the SWCNT(5,5) is unable to hold the $Au_3(ApU)$/A compartment hence DNA probe can not be constructed from SWCNT(5,5)/$Au_3(ApU)$/A complex. The Au10 atom in both SWCNTs/$Au_3(ApU)$ complexes, which holding the positive charge, is very reactive to bind with N7 anchor point in adenine base due to an existence of lone pair electrons. Owing to the intermolecular interaction in SWCNT/$Au_3(ApU)$ complex is not strong enough, the Au_3/A in SWCNT/$Au_3(ApU)$/A moves away from SWCNT. Although, the SWCNT(8,0)/$Au_3(ApU)$ is very stable, but the competitive affinity effects not only to diminish the interaction between SWCNT and Au_3 but also to incommode the Au10-N7 bond formation. According to Mulliken population analysis, the direction of electrons flow in SWCNT(8,0)/$Au_3(ApU)$/A is similar to that in SWCNT(8,0)/Au/A system by losing electrons from adenine recognition molecule to SWCNT(8,0) /$Au_3(ApU)$ detection material by 0.197 au. For overall, outcomes in Tables 7 and 8 (Au_3 system) determine that the stability of SWCNT/Au_3/A probe is inferior to Au_3/A.

2.2 Nucleic Acid Sensor Sensitivity

The next discussion concerns the electronic response of SWCNT/gold after analyte adenine detecting. Its sensitivity is compared with the bare gold reference. From previous subsection 2.1, it was noted that the electrons in the adenine base are transferred to all types of supports, even to poor adenine adsorption. The

electronic sensitivity analysis is the monitoring of the energy gap modulation including the electron transfer characteristic. The SWCNT/Au hybrid sensing material can induce electrons from the adenine base with more power than the Au bare sensing material can (by around 0.1 au.). The trends of energy gap modulation in Au and SWCNT(8,0)/Au complexes when capturing the adenine base are contrary, which increases in the Au/A probe (by 0.13 eV) and decreases in the SWCNT(8,0)/Au/A probe (by -0.03 eV). These events infer that the electron transfer rate in the SWCNT(8,0)/Au/A system is enhanced and is also greater than in the Au/A complexes due to the energy gap of SWCNT(8,0)/Au/A being less (cf. in Table 6). The SWCNT(5,5)/Au complex is insensitive to energy gap changing, but it can induce the electron transfer from the adenine base with better capability than the Au single atom. From the overall results, the Au single atom and SWCNT(8,0)/Au hybrid material provide different characteristics of the electronic signal. After binding with the adenine molecule, the electrical flow in the Au sensing system decreases (more resistance), while in the SWCNT(8,0)/Au one it increases (more conductance). However, we would like to assume that, for the electrical flow aspects, the SWCNT(8,0)/Au system is more practical than the bare Au system due to the target electrons being moved faster to the sensing device, and it also has more capability of adenine capturing.

The Au_3 (IP and PP), SWCNT(8,0)/Au_3(ApD) and SWCNT(8,0)/Au_3(ApU) complexes have the same situation as with the Au complex where the energy gap increases after combining with the adenine molecule, by 0.47 eV, 0.08 eV and 0.07 eV, respectively (cf. in Tables 6 and 7), so they are unable to accelerate these electrons for signal processing. Unlike the stable complexes of SWCNT(5,5)/Au_3(ApD), the incoming adenine base can improve the conductivity of the system by reducing the energy gap by -0.16 eV. Nevertheless, there is a greater possibility that the Au_3 cluster moves away from SWCNT(5,5) to combine with the incoming adenine base. Hence, for electrical resistance detection, the Au_3 sensing system is probably more suitable than the SWCNT(8,0)/Au_3 one.

Table 9 The important geometrical parameters and Mulligen atomic charges of adenine (as reference) base and several adenine probes; Au/A, $Au_3(IP)/A$, $Au_3(PP)/A$, SWCNT(8,0)/Au/A, SWCNT(5,5)/Au/A, SWCNT/(8,0)$Au_3(ApD)$/A, SWCNT/(5,5)$Au_3(ApD)$/A, SWCNT(8,0/$Au_3(ApU)$/A and SWCNT(5,5/$Au_3(ApU)$/A.

	A	Au/A	$Au_3(IP)/A$	$Au_3(PP)/A$	SWCNT/Au/A		SWCNT/$Au_3(ApD)$/A		SWCNT/$Au_3(ApU)$/A	
					SWCNT(8,0) Complex	SWCNT(5,5) Complex	SWCNT(8,0) Complex	SWCNT(5,5) Complex	SWCNT(8,0) Complex	SWCNT(5,5) Complex
Distance (Å)										
r (N6·H6′)	1.01	1.01	1.01	1.01	1.01	1.01	1.01	1.01	1.01	1.01
r (N6·H6″)	1.01	1.02	1.02	1.02	1.02	1.02	1.02	1.03	1.02	1.02
r (N6·Au)[a]	-	3.40	3.64	3.40	3.43	3.44	3.56	3.50	3.47	3.37
Angle (degree)										
∠(C6N6H6′)	119.1	118.7	117.6	118.4	118.5	118.6	117.5	117.6	118.5	118.4
∠(C6N6H6″)	120.1	120.1	123.2	121.2	120.9	120.8	123.3	123.5	120.9	121.0
Charge (au.)										
q_M (N7)	-0.208	-0.307	-0.336	-0.346	-0.256	-0.253	-0.300	-0.294	-0.306	-0.342
q_M (C5)	-0.032	0.071	0.064	0.076	0.060	0.054	0.046	0.047	0.057	0.075
q_M (C6)	0.112	0.116	0.132	0.127	0.125	0.130	0.128	0.116	0.122	0.125
q_M (N1)	-0.189	-0.180	-0.183	-0.181	-0.172	-0.181	-0.181	-0.182	-0.179	-0.181
q_M (N6)	-0.184	-0.185	-0.178	-0.182	-0.178	-0.186	-0.171	-0.163	-0.188	-0.183
q_M (H6′)	0.143	0.150	0.156	0.159	0.154	0.157	0.146	0.145	0.156	0.156
q_M (H6″)	0.159	0.171	0.161	0.185	0.177	0.179	0.160	0.161	0.183	0.187

[a] N6·Au10 and N6H6″Au10 in Au $Au_3(PP)$ and SWCNT/$Au_3(ApU)$ systems

2.3 Prophecy for Thymine Hybridization

This topic is related to the information in Table 9 which elaborates the key parameters of the adenine base in all probe structures. The fact that those Au, Au$_3$, SWCNT/Au and SWCNT/Au$_3$ complexes act as electron withdrawing components. Even though the adenine base acquires positive charges as the consequence of interactions (such as C5 and C6 having more positive charges) but the N7 atoms in those complexes possessing the more negative charges compared with the isolated adenine bases value. The N7 atom gains electrons in order to compensate for the considerable electron loss. On interactions of the adenine base with Au, Au$_3$, SWCNT/Au and SWCNT/Au$_3$, the N1 atoms (the position of the hydrogen bond forming with the H3 proton of the thymine base) hold less negative charges. The electrophilic protons at H6′ positions hold more positive charges. Moreover, the ∠(C6N6H6') values are slightly decreased in readiness for the exocyclic N6H6′ bond to bind with the O4 atom of the thymine molecule. These findings guide us to the prophesy that , Au$_3$, SWCNT/Au and SWCNT/Au$_3$ will cause a weaker hydrogen bonding at the N1 position and a stronger hydrogen bonding at N6-H6′. The interactions of Au, Au$_3$, SWCNT/Au and SWCNT/Au$_3$ with the adenine base make the N6-H6″ bond lengthen by 0.01 Å and also widen the ∠(C6N6H6″).
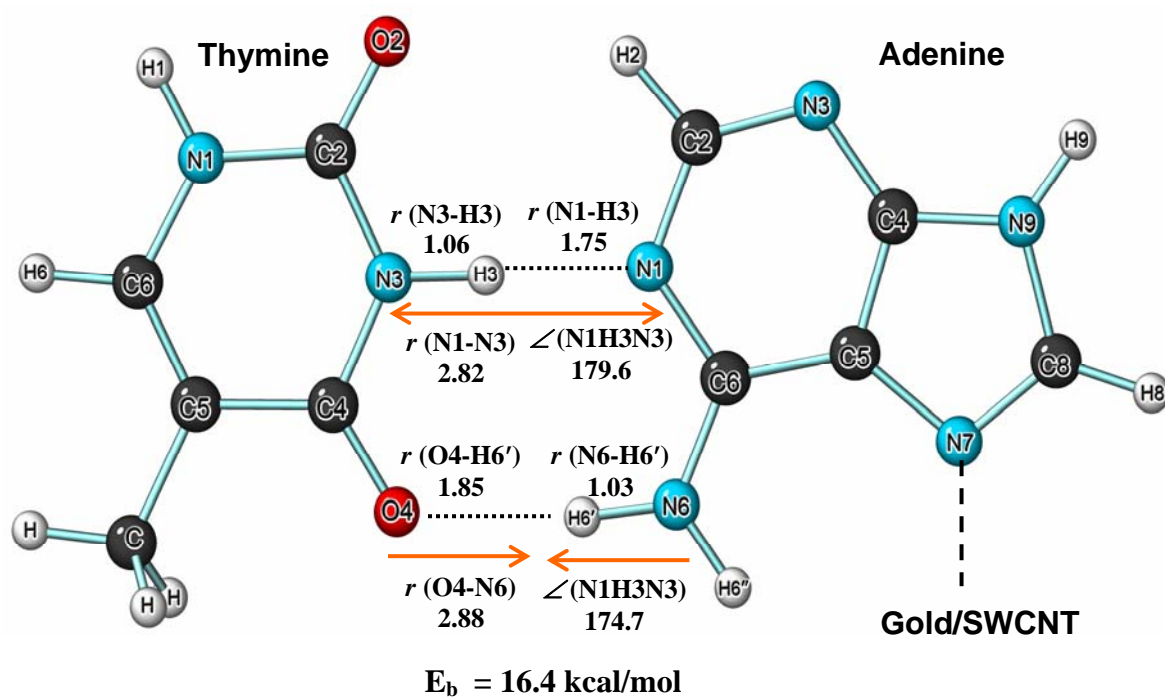
Figure 24 The geometry of double hydrogen bond of original A:T base pair (as reference) and calculated binding energies (E_b). The arrows show the trend of changing N3-H3···N1 and O4···H6′-N6 hydrogen bonds after binding with gold or SWCNT/gold complexes.

Table 10 The geometrical parameters, Mulligen atomic charges and calculated binding energies (E_b) of double hydrogen bond of original A:T base pair (as reference) and several target-probe systems.

	A:T	Au/A:T	Au$_3$(IP)/A:T	Au$_3$(PP)/A:T	SWCNT/Au/A:T		SWCNT/Au$_3$(ApD)/A:T		SWCNT/Au$_3$(ApU)/A:T	
					SWCNT(8,0) Complex	SWCNT(5,5) Complex	SWCNT(8,0) Complex	SWCNT(5,5) Complex	SWCNT(8,0) Complex	SWCNT(5,5) Complex
Distance (Å)										
r (N1·N3)	2.82	2.84	2.85	2.85	2.86	2.85	2.86	2.86	2.84	-
r (N1·H3)	1.75	1.78	1.80	1.80	1.81	1.80	1.80	1.80	1.78	-
r (N3·H3)	1.06 (1.02)^a	1.06	1.06	1.06	1.05	1.06	1.06	1.06	1.06	-
r (O4·N6)	2.88	2.87	2.87	2.84	2.83	2.84	2.84	2.86	2.88	-
r (O4·H6′)	1.85	1.84	1.83	1.80	1.79	1.80	1.81	1.83	1.84	-
r (N6·H6′)	1.03	1.03	1.04	1.04	1.04	1.04	1.04	1.03	1.04	-
Angle (degree)										
∠(N1H3N3)	179.6	179.3	178.9	178.6	178.1	178.6	178.6	178.3	179.2	-
∠(O4H6′N6)	174.7	176.1	177.5	177.3	177.7	177.0	178.7	177.8	176.0	-
∠(C6N6H6′)	120.7	120.2	119.7	120.0	120.3	120.2	119.8	119.6	120.0	-
∠(C6N6H6″)	118.4	118.6	121.0	119.5	119.2	119.2	121.2	121.4	119.4	-
Charge (au.)										
q_M (N1)	-0.207	-0.200	-0.213	-0.211	-0.205	-0.199	-0.203	-0.206	-0.201	-
q_M (N6)	-0.199	-0.209	-0.181	-0.194	-0.208	-0.210	-0.199	-0.190	-0.203	-
q_M (H6′)	0.180	0.184	0.190	0.186	0.188	0.190	0.192	0.194	0.189	-
q_M (H6″)	0.150	0.167	0.148	0.176	0.181	0.178	0.148	0.151	0.173	-
q_M (O4)	-0.354 (-0.290)^a	-0.352	-0.346	-0.351	-0.346	-0.347	-0.342	-0.341	-0.350	-
q_M (N3)	-0.076 (-0.050)^a	-0.078	-0.070	-0.069	-0.076	-0.066	-0.067	-0.070	-0.073	-
q_M (H3)	0.153 (0.141)^a	0.149	0.157	0.157	0.157	0.148	0.149	0.155	0.155	-
E$_b$ (A:T) kcal/mol	16.4	15.8	15.2	15.8	15.5	16.0	15.2	14.8	15.7	-

3. SWCNT/Gold/Adenine:Thymine Complexes (Target Capture)

The final step in DNA sensor development is evaluating of system stability (probe strand and analyte-target binding) and electronic sensitivity. The DNA sensor performances of gold and SWCNT/gold supporters is monitored and clearly expounded in this chapter. The overall outputs are depicted and detailed in Figure 24 and Table 10.

3.1 Stability

The binding of thymine with adenine slightly perturb both the adenine-gold and the gold-SWCNT interactions in all cases. Therefore, the all Au/A:T, Au_3/A:T , SWCNT/Au/A:T and SWCNT/Au_3/A:T complexes maintain the stability of probe strands acting as electronic delivery part. Surprisingly, in all SWCNT/Au/A:T complexes, the A:T base pairs always arrange in a perpendicular direction to the SWCNTs alignments even though the C_S symmetry constraint was not applied (cf. in Figure 21). The cyclic hydrogen bonds analysis in isolated A:T base pair shows two significant electron transfer interactions. The first one is an electron transfer from a lone orbital of the N1 atom in adenine to a N3-H3 antibonding orbital in the thymine base (N3-H3 bond is lengthened by 0.04Å) and the second one is an electron transfer from the lone orbital of the O4 atom in thymine to a N6-H6' antibonding orbital in adenine molecule (N6-H6' bond is lengthened by 0.02Å). From structural study of isolate A:T base pair (Table 10), the r (N1-N3) is shorter than r (O4-N6) and the $\angle$(N1H3N3) bond angle is closer to the optimum interaction alignment of 180° than $\angle$(O4H6'N6). These outcomes refer that, the strength of N1···H3-N3 interaction is greater than that of the O4···H6-N6 interaction.

For revealing the effects of the Au atom, Au_3 cluster, SWCNT/Au and SWCNT/Au_3 on the A:T base pair, Figure 24 and Table 10 show optimized geometrical parameters in the double hydrogen bonds region of A:T base pair complexes. It is noted that the gold atom causes a weaker N3-H3···N1 hydrogen bond, and is even much weaker when the gold atom is attached on a sidewall of the SWCNT.

The distances between N3 and N1 in the N3-H3···N1 hydrogen bond are 2.82, 2.84, 2.86 and 2.85 Å for A:T, Au/A:T, SWCNT(8,0)/Au/A:T and SWCNT(5,5)/Au/A:T systems, respectively. There are resembling alterations in A:T, Au$_3$(IP)/A:T, SWCNT(8,0)/Au$_3$(ApD)/A:T and SWCNT(5,5)/Au$_3$(ApD)/A:T series by increasing of the N1-N3 distance from 2.82 to 2.85, 2.86 and 2.86 Å, respectively and whereas in SWCNT(8,0)/Au$_3$(ApU)/A:T is just 2.84 Å. The lengthened N1-N3 bonds are corresponding with the increasing of N1-H3 bond distance and the decreasing of N3-H3 bond distance. However, the findings in the O4···H6′-N6 hydrogen bond are in an opposite way to that in the N3-H3···N1 one. The O4-N6 distance is shortened from 2.88 Å to 2.87, 2.83 and 2.84 Å via interactions of the base pair with Au, SWCNT(8,0)/Au and SWCNT(5,5)/Au, respectively. There is the same trend but less impact action from Au$_3$ cluster deposited on SWCNT. The O4-N6 bond is contracted from 2.88 Å to 2.84 and 2.86 Å in SWCNT(8,0)/Au$_3$(ApD)/A:T and SWCNT(5,5)/Au$_3$(ApD)/A:T complexes, respectively while this bond in SWCNT(8,0)/Au$_3$(ApU)/A:T complex is unperturbed. Again, the shortened O4-N6 bonds are corresponding with the increasing of N6-H6' bond distance and the decreasing of O4-H6' bond distance. For Mulliken charges analysis when compare with isolate A:T base pair, the interaction of gold and SWCNT/gold with the adenine base causes the electron loss in the adenine molecule (more positive charge) consequently, it retards the electron transfer from the adenine to thymine molecule (less negative charge) ,as detailed in Tables 6, 7,and 8.

The comparisons of binding and total binding energies, it is found that most of the binding energies exhibited corresponding with the bond length modulations. The interactions of A:T base pairs are weakened from 16.4 kcal/mol to 15.8, 15.5 and 16.0 kcal/mol for Au/A:T, SWCNT(8,0)/Au/A:T and SWCNT(5,5)/Au/A:T complexes, respectively. The more reactive mode of Au$_3$ cluster, Au$_3$(IP), significantly reduces the A:T interaction from 16.4 kcal/mol to 15.2, 15.2 and 14.8 kcal/mol for Au$_3$(IP)/A:T, SWCNT(8,0)/Au$_3$(ApD)/A:T and SWCNT(5,5)/Au$_3$(ApD)/A:T, respectively. There is a small change of A:T interaction in Au$_3$(PP)/A:T and SWCNT(8,0)/Au$_3$(ApU)/A:T where the binding energy is decreasing to 15.8 and 15.7 kcal/mol. The minute destabilization of the base pair (by 0.4-1.6 kcal/mol) can be

justified by a compensation between a weakening of N3-H3···N1 bond (bond shrinking and angle adjusting away from 180°) and a strengthening of O4-H6′···N6 bond (bond stretching and angle adjusting close to 180°) in the A:T base pair.

3.2 Sensitivity

We compare the information in Tables 6, 7 and 8 for explanation the electronic communication aspect. After SWCNT/Au/A or Au/A probes are hybridized with the thymine molecule, we cannot observe explicit changes of the energy gaps. However, a general electronic sensing devices base on changing in electrical conductance but they are also restricted by other important factors such as their incapability to recognize with low binding energies and poor charge transfers to transducers. The DNA sensor probes (SWCNT/Au/A) can provide the electronic responses after the hybridization with the thymine molecule which can be elucidated from the modulation of SWCNT/Au/A charges which are defined as the Δq_{Mprobe} parameter (cf. in Table 11).

$$\Delta q_{Mprobe}(Au_n/A) = q_M(Au_n/A) \text{ in } [Au_n/A:T] - q_M(Au_n/A) \text{ in } [Au_n/A] \qquad (7)$$

$$\Delta q_{Mprobe}(SWCNT/Au_n/A) = q_M(Au_n/A) \text{ in } [SWCNT/Au_n/A:T]$$
$$- q_M(SWCNT/Au_n/A) \text{ in } [SWCNT/Au_n/A] \qquad (8)$$

Table 11 The Δq_{Mprobe} and $\Delta q_{Msupport}$ (au.) parameters of Au/A:T, Au$_3$(IP)/A:T, Au$_3$(PP)/A:T, SWCNT(8,0)/Au/A:T, SWCNT(5,5)/Au/A:T, SWCNT(8,0)/Au$_3$(ApD)/A:T, SWCNT(5,5)/Au$_3$(ApD)/A:T, SWCNT(8,0)/Au$_3$(ApU)/A:T, SWCNT(5,5)/Au$_3$(ApU)/A:T complexes.

	Au/A:T	Au$_3$(IP)/A:T	Au$_3$(PP)/A:T	SWCNT/Au/A:T		SWCNT/Au$_3$(ApD)/A:T		SWCNT/Au$_3$(ApU)/A:T	
				SWCNT (8,0)]Complex	SWCNT (5,5) Complex	SWCNT (8,0) Complex	SWCNT (5,5) Complex	SWCNT (8,0) Complex	SWCNT (5,5) Complex
Δq_{Mprobe} (au.)	0.032	0.017	0.013	0.010	0.017	0.020	0.026	0.025	-
$\Delta q_{Msupport}$ (au.)	-0.002	-0.005	0.000	-0.004	-0.008	-0.004	-0.006	-0.004	-

The greater value of Δq_{Mprobe} likely corresponds with the higher sensitivity material. However, both the equations mean that the counter balance (compensation effect) of the charge gaining and losing with the thymine molecule. All the positive values of the Δq_{Mprobe} parameter infer that the main contribution effect is the electrons transferring to the thymine molecule. Nevertheless, there are some electrons moving from the thymine molecule to the adenine probe and these electrons are continuously transferred to support and be processed to be the output signal. Therefore, the parameter Δq_{Mprobe} is meaningless for electronic response observation. Accordingly, we prefer to study the alteration of SWCNT/Au charges in SWCNT/Au/A and SWCNT/Au/A which give the better electronic sense. The charge alterations which also represent the amount of sensor signals are defined as follow:

$$\Delta q_{Msupport}(Au_n) = q_M(Au_n) \text{ in } [Au_n/A:T] - q_M(Au_n) \text{ in } [Au_n/A] \qquad (9)$$

$$\Delta q_{Msupport}(SWCNT/Au_n) = q_M(SWCNT/Au_n) \text{ in } [SWCNT/Au_n/A:T]$$
$$- q_M(SWCNT/Au_n) \text{ in } [SWCNT/Au_n/A] \qquad (10)$$

All values of $\Delta q_{Msupport}$ are tabulated in Table 11. The $\Delta q_{Msupport}(SWCNT(8,0)/Au)$ and $\Delta q_{Msupport}(SWCNT (5,5)/Au)$ are evaluated to be -0.004 au. and -0.008 au., respectively while the $\Delta q_{Msupport}(Au)$ is just -0.002 au. Therefore, the SWCNT/Au integrated probe has greater efficiency to amplify the electronic signal than the bare gold atom. The sensing response in $Au_3(PP)$ system is unmeasurable because of the zero $\Delta q_{Msupport}(Au_3)$ value. While, the $Au_3(IP)$ system is able to provide the acceptable signal with $\Delta q_{Msupport}(Au_3)$ is equal to -0.005 au. In accordance with the sensing quality, the $Au_3(IP)/A$ probe perform sensor capability as well as SWCNT(8,0)/Au_3(ApD)/A and SWCNT(5,5) /Au_3(ApD)/A do, with modulating the signal by around -0.005 au. of $\Delta q_{Msensor}$. Hence, there are the same situations as found in SWCNT/Au/A probe which behaves insensitive electronic conductance changing (after hybridization) but it still enhances the electron transfers to the detection part. For the SWCNT(8,0)/Au_3(ApU)/A:T system, the hybridization also induces the conductivity changing which can be observed by the energy gap decreasing from 0.09 to 0.06 eV. Therefore the nucleic acid immobilization in the SWCNT(8,0)/

$Au_3(ApU)/A$ is weaker than that in the $Au_3(PP)/A$ probe but it still offers the better electronic response.

4. Preliminary Summarization

The effectiveness in development of SWCNT/gold-based DNA sensor is achieved as follows: (1) substantial stability of DNA probe immobilization; (2) measurable electrical signature of the target detection (distinct charge transfer or sensitive conductivity); (3) robustness of DNA hybridization. Both of SWCNT(8,0)/Au and SWCNT(5,5)/Au materials have all those three properties with similar ability and their performance is better than the bare Au atom's. However, the obstacle concerning the stability of the DNA probe structure causes a difficulty to the accomplishment in SWCNT/Au$_3$ systems. The immobilization of adenine on the SWCNTN/Au$_3$ transducer is not only worse than that on the Au$_3$ bare cluster but also causes a destabilization in the SWCNTN/Au$_3$ combination structure. Especially, the SWCNT(5,5)/Au$_3$(ApU) complex is ruined. Moreover, SWCNT(8,0)/Au$_3$(ApD) and SWCNT(5,5)/Au$_3$(ApD) complexes are destabilized by the integration with adenine base. For the stability point of view, the most stable SWCNT/Au$_3$ structure of each SWCNT type is the most suitable for the adenine probe construction. The very stable complex of SWCNT(8,0)/Au$_3$ series is the SWCNT(8,0)/Au$_3$(ApU). Even though it is not good for the adenine immobilization, it controls the elongation of SWCNT$\cdots$Au$_3$ distance. Additionally, the SWCNT(8,0)/Au$_3$(ApU)/A receptor is electrical conductance that is sensitive to the target thymine molecule and it also provides the detectable signal (-0.005 au.). Finally, the most powerful hybridization is found in the SWCNT(8,0) /Au$_3$(ApU)/A:T complex as compared with the other SWCNT/Au$_3$/A:T systems. All above expressions let us to suggest that the semiconductor SWCNT(8,0) is more appropriate to produce the SWCNT/gold-base DNA sensor than the metallic SWCNT(5,5).

CONCLUSION

By performing the DFT calculation on complexes of SWCNT/Au/A:T and SWCNT/Au$_3$/A:T with both SWCNT(8,0) and SWCNT(5,5) and their sub systems, the overall outcomes guide us to conclude that the SWCNT/Au hybrid structure has a superior sensor performance to the conventional gold probe due to the electron gaining characteristics of the alternative integrated materials. The other interesting function of the SWCNT/Au hybrid structure beyond acting as the platform for the adenine probe construction is that it is the sensing material for nucleic acids. The SWCNT/Au structure is more reactive to adenine capturing than is the Au atom, by gaining more electrons. Especially, the SWCNT(8,0)/Au/A complex can accelerate electrons to transfer to the sensing part. However, the binding of A:T with SWCNT/Au$_3$ hetero structure is weaker than that with the bare Au$_3$ cluster. The SWCNT/Au$_3$ contact diminishes the binding of the A:T base pair. This alteration is attributed to the occurrence of the competitive affinity in the ApU deposite mode and the nonconventional hydrogen bonding in the ApD one. Nevertheless, the stable structures of SWCNT(8,0)/Au$_3$ and SWCNT(5,5)/Au$_3$ still provide the acceptable sensing performance. The electron withdrawing property of Au atom, Au$_3$ cluster, SWCNT/Au and SWCNT/Au$_3$ causes a contraction of the N3-H3$\cdots$N1 hydrogen bond and a stretching of O4-H6'$\cdots$N6 one. However, the hydrogen bond alteration is insufficient to cause the A:T base pair destabilization. The present study is intended to provide useful information that can be applied to developing the SWCNT as a novel candidate in a DNA detector.

LITERATURE CITED

Ahlrichs, R., M. Baer, M. Haeser, H. Horn and C. Koelmel. 1989. Electronic structure calculations on workstation computers: the program system TURBOMOLE. **Chemical Physics Letters** 162(3):165-169.

Bravo-Perez, G., I.L. Garzon and O. Novaro. 1999. Ab initio study of small gold clusters. **Theochem** 493225-231.

Cai, H., X. Cao, Y. Jiang, P. He and Y. Fang. 2003. Carbon nanotube-enhanced electrochemical DNA biosensor for DNA hybridization detection. **Analytical and Bioanalytical Chemistry** 375(2):287-293.

Carter T., W. and M. John W. 2005. Fundamental Properties of Single-Wall Carbon Nanotubes. **Journal of Physical Chemistry B** 109(1):52-65.

Chen, J., Y. Miao, N. He, X. Wu and S. Li. 2004. Nanotechnology and biosensors. **Biotechnology Advances** 22(7):505-518.

Daniel, M.-C. and D. Astruc. 2004. Gold Nanoparticles: Assembly, Supramolecular Chemistry, Quantum-Size-Related Properties, and Applications toward Biology, Catalysis, and Nanotechnology. **Chemical Reviews (Washington, DC, United States)** 104(1):293-346.

Demers, L.M., M. Oestblom, H. Zhang, N.-H. Jang, B. Liedberg and C.A. Mirkin. 2002. Thermal Desorption Behavior and Binding Properties of DNA Bases and Nucleosides on Gold. **Journal of the American Chemical Society** 124(38):11248-11249.

Dimitrios, T., T. Nikos, B. Alberto and P. Maurizio. 2006. Chemistry of Carbon Nanotubes. **Chemical Review.** 106(3):1105-1136.

Drummond, T.G., M.G. Hill and J.K. Barton. 2003. Electrochemical DNA sensors. **Nature Biotechnology** 21(10):1192-1199.

Durgun, E., S. Dag, V.M.K. Bagci, O. Gulseren, T. Yildirim and S. Ciraci. 2003. Systematic study of adsorption of single atoms on a carbon nanotube. **Physical Review B: Condensed Matter and Materials Physics** 67(20):201401/201401-201401/201404.

Eichkorn, K., O. Treutler, H. Oehm, M. Haeser and R. Ahlrichs. 1995. Auxiliary basis sets to approximate Coulomb potentials. [Erratum to document cited in CA123:93649]. **Chemical Physics Letters** 242(6):652-660.

Gao, H. and Y. Kong. 2004. Simulation of DNA-nanotube interactions. **Annual Review of Materials Research** 34123-150.

Gruner, G. 2006. Carbon nanotube transistors for biosensing applications. **Analytical and Bioanalytical Chemistry** 384(2):322-335.

Hongjie, D. 2002. Carbon Nanotubes: Synthesis, Integration, and Properties. **Accounts of Chemical Research** 35:1035-1044.

Jiang, L. and L. Gao. 2003. Modified carbon nanotubes: an effective way to selective attachment of gold nanoparticles. **Carbon** 41(15):2923-2929.

Kimura-Suda, H., D.Y. Petrovykh, M.J. Tarlov and L.J. Whitman. 2003. Base-Dependent Competitive Adsorption of Single-Stranded DNA on Gold. **Journal of the American Chemical Society** 125(30):9014-9015.

Kryachko, E.S. and F. Remacle. 2005a. Complexes of DNA Bases and Gold Clusters Au3 and Au4 Involving Nonconventional N-H...Au Hydrogen Bonding. **Nano Letters** 5(4):735-739.

Kryachko, E.S. and F. Remacle. 2005b. Complexes of DNA Bases and Watson-Crick Base Pairs with Small Neutral Gold Clusters. **Journal of Physical Chemistry B** 109(48):22746-22757.

Lim, S.H., J. Wei and J. Lin. 2004. Electrochemical genosensing properties of gold nanoparticle-carbon nanotube hybrid. **Chemical Physics Letters** 400(4-6):578-582.

Liu, L., T. Wang, J. Li, Z.-X. Guo, L. Dai, D. Zhang and D. Zhu. 2002. Self-assembly of gold nanoparticles to carbon nanotubes using a thiol-terminated pyrene as interlinker. **Chemical Physics Letters** 367(5,6):747-752.

Ma, X., X. Li, N. Lun and S. Wen. 2006. Synthesis of gold nano-catalysts supported on carbon nanotubes by using electroless plating technique. **Materials Chemistry and Physics** 97(2-3):351-356.

Merkoci, A. 2006. Carbon nanotubes in analytical sciences. **Microchimica Acta** 152(3-4):157-174.

Merkoci, A., M. Pumera, X. Llopis, B. Perez, M. del Valle and S. Alegret. 2005. New materials for electrochemical sensing VI: Carbon nanotubes. **TrAC, Trends in Analytical Chemistry** 24(9):826-838.

Natalia, C., Tansil and G. Zhiqiang. 2006. Nanoparticles in biomolecular detection. **Nanotoday** 1(1):28-37.

Patolsky, F. and C.M. Lieber. 2005. Nanowire nanosensors. **Materials Today (Oxford, United Kingdom)** 8(4):20-28.

Perdew, J.P., K. Burke and M. Ernzerhof. 1996. Generalized gradient approximation made simple. **Physical Review Letters** 77(18):3865-3868.

Portney, N.G. and M. Ozkan. 2006. Nano-oncology: drug delivery, imaging, and sensing. **Analytical and Bioanalytical Chemistry** 384(3):620-630.

Riu, J., A. Maroto and F.X. Rius. 2006. Nanosensors in environmental analysis. **Talanta** 69(2):288-301.

Roco, M.C. 2003. Nanotechnology: convergence with modern biology and medicine. **Current Opinion in Biotechnology** 14(3):337-346.

Rogers, K.R. 2006. Recent advances in biosensor techniques for environmental monitoring. **Analytica Chimica Acta** 568(1-2):222-231.

Shukla, R., V. Bansal, M. Chaudhary, A. Basu, R.R. Bhonde and M. Sastry. 2005. Biocompatibility of Gold Nanoparticles and Their Endocytotic Fate Inside the Cellular Compartment: A Microscopic Overview. **Langmuir** 21(23):10644-10654.

Sigel, H. 1993. Interactions of metal ions with nucleotides and nucleic acids and their constituents. **Chemical Society Reviews** 22(4):255-267.

Song, C., Y. Xia, M. Zhao, X. Liu, F. Li and B. Huang. 2005. Ab initio study of base-functionalized single walled carbon nanotubes. **Chemical Physics Letters** 415(1-3):183-187.

Sun, Y. and C.-H. Kiang. 2005. DNA-based artificial nanostructures: fabrication, properties, and applications. **Handbook of Nanostructured Biomaterials and Their Applications in Nanobiotechnology** 2223-247.

Thaxton, C.S., D.G. Georganopoulou and C.A. Mirkin. 2006. Gold nanoparticle probes for the detection of nucleic acid targets. **Clinica Chimica Acta** 363(1-2):120-126.

Trojanowicz, M. 2006. Analytical applications of carbon nanotubes: a review. **TrAC, Trends in Analytical Chemistry** 25(5):480-489.

Valcarcel, M., B.M. Simonet, S. Cardenas and B. Suarez. 2005. Present and future applications of carbon nanotubes to analytical science. **Analytical and Bioanalytical Chemistry** 382(8):1783-1790.

Vaseashta, A. and D. Dimova-Malinovska. 2005. Nanostructured and nanoscale devices, sensors and detectors. **Science and Technology of Advanced Materials** 6(3-4):312-318.

Vercoutere, W. and M. Akeson. 2002. Biosensors for DNA sequence detection. **Current Opinion in Chemical Biology** 6(6):816-822.

Wang, J. 2002. Electrochemical nucleic acid biosensors. **Analytica Chimica Acta** 469(1):63-71.

Watson, J.D. and F.H.C. Crick. 1953. Molecular structure of nucleic acids. A structure for deoxyribose nucleic acid. **Nature (London, United Kingdom)** 171737-738.

Wells, D.H., W.N. Delgass and K.T. Thomson. 2004. Formation of hydrogen peroxide from H2 and O2 over a neutral gold trimer: a DFT study. **Journal of Catalysis** 225(1):69-77.

Zhai, J., C. Hong and R. Yang. 1997. DNA based biosensors. **Biotechnology Advances** 15(1):43-58.

Zhang, Y., N. W., Franklin, R.J. Chen and H. Dai. 2000. Metal coating on suspended carbon nanotubes and its implication to metal-tube interaction. **Chemical Physics Letters** 33135-41.

Zhang, Z.-L., D.-W. Pang, H. Yuan, R.-X. Cai and H.D. Abruna. 2005. Electrochemical DNA sensing based on gold nanoparticle amplification. **Analytical and Bioanalytical Chemistry** 381(4):833-838.

APPENDIX

Appendix: Theoretical Background

Theory of Quantum Chemical Calculations

Quantum mechanical methods for the study of molecules can be divided into two categories: *ab initio* and semiempirical models. *Ab initio* methods refer to quantum chemical methods in which all the integrals are exactly evaluated in the course of a calculation. *Ab initio* methods include Hartree-Fock (HF) or molecular orbital (MO) theory, configuration interaction (CI) theory, perturbation theory (PT), and density functional theory (DFT). *Ab initio* methods that include correlation have accuracy comparable with experiment in structure and energy predictions. However, a drawback is that *ab initio* calculations are extremely demanding in computer resources, especially for large molecular systems. Semiempirical quantum chemical methods lie between *ab initio* and molecular mechanics (MM). Like MM, they use experimentally derived parameters to strive for accuracy; like *ab initio* methods, they are quantum-mechanical in nature. Semiempirical methods are computationally fast because many of the difficult integrals are neglected. The error introduced is compensated through the use of parameters. Thus, semiempirical procedures can often produce greater accuracy than *ab initio* calculations at a similar level.

1. Schrödinger Equation

The quantum chemical methods are based on finding solutions to the Schrödinger equation on molecular orbital theory. According to quantum mechanics postulates, the state of a system is fully described by a wave function that depends on the position of the electrons and nuclei in the system.

$$H\Psi = E\Psi \tag{1}$$

where H is the Hamiltonian operator which gives the kinetic, T, and potential, V, energies of the system that is;

$$H = T + V \tag{2}$$

and

$$T = -\frac{\hbar^2}{2m} \nabla^2 \tag{3}$$

then

$$H = -\frac{\hbar^2}{2m} \nabla^2 + V \tag{4}$$

Then, rewrite equation (1) is;

$$\left\{ -\frac{\hbar^2}{2m} \nabla^2 + V \right\} \Psi = E\Psi \tag{5}$$

where the Laplacian operator, ∇^2, is ;

$$\nabla^2 = \frac{\partial^2}{\partial x^2} + \frac{\partial^2}{\partial y^2} + \frac{\partial^2}{\partial z^2} \tag{6}$$

$\hbar$ is Plank's constant divided by 2π. Ψ is the wave function which characterizes the particle's properties. E is the eigen energy of the particle corresponding to wave function.

2. Born-Oppenheimer approximation

Now consider N particle system, the Hamiltonian operator (H), is composed of two parts, the kinetic (T) and potential (V) energy part which describes the electron (in atomic units) as shown in equation (2) so:

$$H = -\sum_{i=1}^{N} \frac{1}{2} \nabla_i^2 - \sum_{A=1}^{M} \frac{1}{2M_A} \nabla_A^2 - \sum_{i=1}^{N} \sum_{A=1}^{M} \frac{Z_A}{r_{iA}} + \sum_{i=1}^{N} \sum_{j>i}^{N} \frac{1}{r_{ij}} + \sum_{A=1}^{M} \sum_{B>A}^{M} \frac{Z_A Z_B}{R_{AB}} \tag{7}$$

The Hamiltonian can thus be separated into two main parts, which is one operator to describe the electron and the other to describe the nucleus.

$$\text{H} = -\sum_{A=1}^{M} \frac{1}{2M_A} \nabla_A^2 + \text{H}_{el} \tag{8}$$

This focus on the electronic Hamiltonian, H_{el}, and try to solve the electronic Schrödinger equation in the field of the fixed nuclei. The nuclear-nuclear repulsion term (the final in equation (7)) appears as a constant in H_{el}. Further assume the wave function $\psi(\vec{r}, \vec{R})$ to be a product of an electronic and a nuclear part:

$$\psi(\vec{r}, \vec{R}) = \psi_{elec}(\vec{r}, \vec{R}) \psi_{nucl}(\vec{R}) \tag{9}$$

The justification for this is that the electrons are much lighter than the nuclei. This is called the Born-Oppenheimer approximation (BO). The parametric $\vec{R}$ dependence of ψ_{elec} arises since the electron distribution depends implicitly on the particular nuclear arrangement for the system under study. The nuclear wave function, ψ_{nucl}, describes the vibrational, rotational and translational motion of the nuclei. From equation (1), (8) and (9) can obtain;

$$\text{H}\psi(\vec{r}, \vec{R}) = \text{H}\psi_{elec}(\vec{r}, \vec{R})\psi_{nucl}(\vec{R}) = \left(-\sum_{A=1}^{M} \frac{1}{2M_A} \nabla_A^2 + \text{H}_{el} \right) \psi_{elec}(\vec{r}, \vec{R})\psi_{nucl}(\vec{R})$$

$$= \left(-\sum_{A=1}^{M} \frac{1}{2M_A} \nabla_A^2 + \text{E}_{el} \right) \psi_{elec}(\vec{r}, \vec{R})\psi_{nucl}(\vec{R}) = \text{E}\psi_{elec}(\vec{r}, \vec{R})\psi_{nucl}(\vec{R}) = \text{E}\psi \tag{10}$$

The electronic wavefunction $\psi_{elec}(\vec{r}, \vec{R})$ can be divided out from both sides of equation (10), provided that terms in $\nabla^2 \psi_{elec}(\vec{r}, \vec{R})$ are small, i.e. the electronic wavefunction changes slowly upon small displacements of the nuclear positions. Thus, if we neglect the influence of the nuclear derivative on the electron wave function

(ψ_{el}) (i.e. the nuclei move slowly compared with the electrons) which can separate equation (10) into two equations, an electronic part:

$$\text{H}_{el}\psi_{el}(\vec{r},\vec{R}) = \text{E}_{el}(\vec{R})\psi_{el}(\vec{r},\vec{R}) \tag{11}$$

where

$$\text{H}_{el} = -\sum_{i=1}^{N}\frac{1}{2}\nabla_i^2 - \sum_{i=1}^{N}\sum_{A=1}^{M}\frac{Z_A}{r_{iA}} + \sum_{i=1}^{N}\sum_{j>i}^{N}\frac{1}{r_{ij}} + \sum_{A=1}^{M}\sum_{B>A}^{M}\frac{Z_A Z_B}{R_{AB}} \tag{12}$$

and a nuclear part:

$$\text{H}_{nucl}\psi_{nucl}(\vec{R}) = \text{E}\psi_{nucl}(\vec{R}) \tag{13}$$

where

$$\text{H}_{nucl} = -\sum_{A=1}^{M}\frac{1}{2M_A}\nabla_A^2 + \text{E}_{el}(\vec{R}) \tag{14}$$

3. Hartree Fock Theory

At this point it is important to mention the Born-Oppenheimer approximation, which states that since the mass of the nuclei is so much greater than the mass of the electron we can consider the nuclei to be stationary with respect to the electron and the kinetic energy term for the nuclei can be neglected. This greatly simplifies the expression. For a complete derivation of this please refer to standard textbooks on this subject. Also, we are neglecting relativistic effects and other operators such as spin-spin coupling effects by using the BO approximation.

Schrödinger equation:

$$\text{H}\psi(\vec{r},\vec{R}) = \text{E}\psi(\vec{r},\vec{R}) \tag{15}$$

An exact solution to the Schrödinger equation is not possible for any but the most trivial molecular systems. However, a number of simplifying assumptions and

procedures do make an approximate solution possible for a large range of molecules. To simplify the treatment further, the next step is to assume that the electrons are non-interacting. This implies that (apart from the constant nuclear-nuclear repulsion term) which can rewrite the total n-electron Hamiltonian as a sum of n one-electron Hamiltonians,

$$H_{el} = \sum_{i=1}^{N} h(i) \tag{16}$$

$$h(i) = \left(-\frac{1}{2} \nabla_i^2 - \sum_{A=1}^{M} \frac{Z_A}{r_{iA}} \right) \tag{17}$$

Through the wave functions, the effective potential is generated. This potential allows to refine wave functions, from which a new potential is obtained. The procedure is repeated until a stable, self-consistent solution is reached. Due to the iterative procedure, the initial guess of the wavefunction, can of course be chosen ad hoc. However, the better the initial guess is, the easier it is to reach a stable solution to the eigenvalue problems in a relatively short computational time, is provided by the variation principle. This can be stated in the following way: Given any approximate wave function, satisfying the correct boundary conditions, the expectation value of the energy obtained by this wave function never lies below the exact energy of the ground state. Expressed in mathematical terms:

$$E_e = \frac{\langle \psi | H_e | \psi \rangle}{\langle \psi | \psi \rangle} \geq E_{exact} \tag{18}$$

A conceptually appealing model for the (trial) wave function of our molecular system is to regard it as being constructed from molecular orbitals (MO). This description in analogous to the model used for the atomic orbitals (AO). The MO's, the elements of the wave function determinant, are in turn thought of as being constructed by a Linear Combination of Atomic Orbitals (LCAO),

$$\psi_i^{MO} = \sum_\mu c_{\mu i}\phi_\mu^{AO} \tag{19}$$

The variational principle leads to following equations describing the molecular orbital expansion coefficients, c_{vi}, derived by Roothaan and by Hall:

$$\sum_{v=1}^{N}\left(F_{\mu v} - \varepsilon_i S_{\mu v}\right)c_{vi} = 0 \quad \mu = 1,2,..., N \tag{20}$$

Equation (16) can be rewritten in matrix form:

$$FC = SC\varepsilon \tag{21}$$

with

$$F_{\mu v} = H_{\mu v}^{core} + \sum_{\lambda\sigma} P_{\lambda\sigma}\left[(\mu v|\lambda\sigma) - \frac{1}{2}(\mu\lambda|v\sigma)\right] \tag{22}$$

$$F_{\mu v} = H_{\mu v}^{core} + G_{\mu v} \tag{23}$$

where $H_{\mu v}^{core}$, core-Hamiltonian matrix, defined as

$$H_{\mu v}^{core} = \int dr_1 \phi_\mu^*(1)h(1)\phi_v(1) \tag{24}$$

The matrix P is the density matrix or charge- and bond-order matrix,

$$P_{\mu v} = 2\sum_{a}^{N/2} C_{\mu a}C_{va}^* \tag{25}$$

The matrix S is the overlap matrix, indicating the overlap between orbitals.

$$S_{\mu v} = \int dr_1 \phi_\mu^*(1) \phi_v(1) \qquad (26)$$

The term $(\mu v | \lambda \sigma)$ in equation 22 signified the two-electron repulsion integrals, defined as

$$(\mu v | \lambda \sigma) = \int dr_1 dr_2 \phi_\mu^*(1) \phi_v(2) r_{12}^{-1} \phi_\lambda^*(1) \phi_\sigma(2) \qquad (27)$$

The (initial) wave function is used to generate an effective potential, which apply this potential in order to refine the coefficient matrix. The modified MO's form the new input in the Roothaan or Pople-Nesbet (1986) equations, and a new potential is generated. The iterative procedure is repeated until convergence is reached, i.e. when the changes in energy and/or charge density in two subsequent iterations are below a pre-set threshold value.

The SCF procedure, outlined is as follows

1. Specify a molecule (a set of nuclear coordinates $\{R_A\}$, atomic numbers $\{Z_A\}$, and number of electron N) and a basis set $\{\phi_\mu\}$.

2. Calculate all required molecular integrals, $S_{\mu v}$, $H_{\mu v}^{core}$ and $(\mu v | \lambda \sigma)$.

3. Diagonalize the overlap matrix S and obtain a transformation matrix X from either equation $X \equiv S^{-1/2} = Us^{-1/2}U^\tau$ or $X = Us^{-1/2}$.

4. Obtain a guess at the density matrix P.

5. Calculate the matrix G of equation $F_{\mu v} = H_{\mu v}^{core} + G_{\mu v}$ from the density matrix P and the two-electron integral $(\mu v | \lambda \sigma)$.

6. Add G to the core-Hamiltonian to obtain the Fock matrix $F = H^{core} + G$.

7. Calculate the transformed Fork matrix $F^\tau = X^\tau F X$

8. Diagonalize F^τ to obtain C' and ε.

9. Calculate $C = XC'$.

10. Form a new density matrix P from C using $P_{\mu v} = 2 \sum_a^{N/2} C_{\mu a} C_{va}^*$.

11. Determine whether the procedure has converged, i.e. determine whether the new density matrix of step (10) is the same as the previous density matrix within a specified criterion. If the procedure has not converged, return to step (5) with the new density matrix.

12. If the procedure has converged, then use the resultant solution, represented by C, P, F, etc., to calculate expectation values and other quantities of interest.

4. Semi-empirical Calculation

Semi-empirical methods increase the speed of computation by using approximations of *ab initio* techniques (*e.g.,* by limiting choices of molecular orbitals or considering only valence electrons) which have been fitted to experimental data. Until recently, the size of many energetic molecules placed them beyond the scope of *ab initio* calculations, so preliminary theoretical studies were performed using semi-empirical techniques. However, semi-empirical methods have been calibrated to typical organic or biological systems and tend to be inaccurate for problems involving hydrogen-bonding, chemical transitions or nitrated compounds.

Because both time and storage requirements of an *ab initio* Hartree-Fock calculation increase as the fourth power of the number of basis functions, calculations on large molecules even with the smallest basis sets are apt to be prohibitive. In such situations, the NDDO (neglect of diatomic differential overlap) formalism affords practical methods for calculating the electronic structure of large systems. Here only one- and two-centre, two-electron integrals are considered, and the Hartree-Fock matrix, consists only of elements for which basis functions μ and ν are on the same atom, and basis functions λ and σ are on another atom. The individual terms are below (the sum α is over all other atoms).

$$F_{\mu\mu} = H_{\mu\mu}^{core} + \sum_{\nu} P_{\nu\nu} \left[\langle \mu\mu | \nu\nu \rangle - \langle \mu\nu | \mu\nu \rangle \right] + \sum_{\delta} \sum_{\lambda} \sum_{\sigma} P_{\lambda\sigma} \langle \mu\mu | \nu\nu \rangle \quad (28)$$

$$F_{\mu\nu} = H_{\mu\nu}^{core} + P_{\mu\nu} \left[3\langle \mu\nu | \mu\nu \rangle - \langle \mu\mu | \nu\nu \rangle \right] + \sum_{\delta} \sum_{\lambda} \sum_{\sigma} P_{\lambda\sigma} \langle \mu\nu | \lambda\sigma \rangle \quad (29)$$

$$F_{\rho\lambda} = \beta_{\rho\lambda} - \frac{1}{2}\sum_{\nu}\sum_{\sigma} P_{\lambda\sigma}\langle\mu\nu|\lambda\sigma\rangle \tag{30}$$

The elimination of three- and four-centre integrals greatly reduces the time and storage requirements for an NDDO calculation (which now increase as the square of the number of atoms) relative to that for a full Hartree-Fock treatment.

Three levels of NDDO theory are included in *SPARTAN'S SEMI EMPIRICAL* module:

- *Modified NDO (MNDO)* a method introduced to correct some of the problems associated with MINDO/3. MNDO does not work well for sterically crowded molecules, four-membered rings, hydrogen bonding, hypervalent compounds, nitro groups and peroxides. In general, MNDO overestimates activation barriers to chemical reactions.

- *Austin Method, version 1 (AM1)* a reparameterised version of MNDO which includes changes in nuclear repulsion terms. Although more accurate than MNDO, AM1 does not handle phosphorus-oxygen bonds, nitro compounds and peroxide bonds.

- *Parameterisation Model, version 3 (PM3)* a second reparameterisation of MNDO, functionally similar to AM1, but with some significant improvements. PM3 is a recently developed semi-empirical method that may contain as yet undiscovered defects.

In all of these formalisms, only the valence electrons are considered. The one electron terms are given by,

$$\mathrm{H}_{\mu\nu}^{core} = U_{\mu\nu} - Z_A \sum_{B\neq A} Z_B \langle\mu\nu|\delta\delta\rangle \tag{31}$$

Here, μ and ν are located on atom A and the summation is over all other atoms. $U_{\nu\nu}$ is related to the binding energy of an electron in atomic orbital ν, and is determined from spectroscopic data. $U_{\nu\mu}$ is set to zero for $\nu \neq \mu$. The second term in equation (31) represents the attraction on an electron on atom A from the nuclear

framework. The two center integral involves only the s function on atom B. Z_A is the charge of atom A without its valence electrons.

All one-centre, two-electron integrals $(\nu\nu|\mu\mu)$ and $(\nu\mu|\nu\mu)$ are fitted to spectroscopic data. The two-centre, two-electron repulsion integrals $(\nu\mu|\lambda\sigma)$ are approximated by classical multipole-multipole charge interactions between atoms A and B. The multipole charge separations within an atom are treated as adjustable parameters, i.e. optimized to fit the experimentally derived one-centre integrals.

The $\beta_{\rho\lambda}$ terms appearing in the Fock matrix (equation (30)) are the one-electron, two-centre core resonance integrals and are approximated as,

$$\beta_{\rho\lambda} = \frac{\beta_\rho + \beta_\lambda}{2} S_{\rho\lambda} \qquad (32)$$

where $S_{\rho\lambda}$ is the overlap integral between Slater orbitals ρ and λ, and $\rho\lambda$ and $\lambda\rho$ are adjustable parameters optimized using experimental thermochemical data for simple molecules. Because all of the adjustable parameters are rooted in experimental data, these methods are known as semi-empirical. As in *ab initio* Hartree-Fock calculations, an SCF procedure is used to converge on a density matrix, and the electronic energy.

The three methods differ only in the core-repulsion terms (they also differ in the detailed parameterization). Core repulsion includes nuclear repulsion and non-valence electron-electron repulsion, which are not explicitly considered in the calculation of the electronic energy. In the MNDO model, the core repulsion energy is given by,

$$E^{CR} = \sum_{A \neq B}\sum_{B \neq A} Z_A Z_B \langle \delta(A) | \delta(B) \rangle \left(e^{-\sigma_a E_{AB}} + e^{-\sigma_B E_{AB}} \right) \qquad (33)$$

In AM1 a sum of Gaussians is employed to better represent the core repulsion behaviour at van der Waals distances. PM3 uses a similar core repulsion function, but differs in the parameterisation procedure.

One advantage of methods parameterised using experimental data is their implicit inclusion of electron correlation effects. However, dependence on experimental data means that semi-empirical methods would not be expected to perform well on unusual types of molecules for which no data are available from which to construct parameters.

5. Density Functional Theory

Density Functional Theory is one of the most popular and successful quantum mechanical approaches to matter. It is nowadays routinely applied for calculating, e.g., the binding energy of molecules in chemistry and the band structure of solids in physics. First applications relevant for fields traditionally considered more distant from quantum mechanics, such as biology and mineralogy are beginning to appear. Superconductivity, atoms in the focus of strong laser pulses, relativistic effects in heavy elements and in atomic nuclei, classical liquids, and magnetic properties of alloys have all been studied with DFT.

DFT owes this versatility to the generality of its fundamental concepts and the flexibility one has in implementing them. In spite of this flexibility and generality, DFT is based on quite a rigid conceptual framework. This section introduces some aspects of this framework in general terms. The following sections then deal in detail with two core elements of DFT, the Hohenberg-Kohn theorem, the Kohn-Sham equations, a (necessarily less detailed) description of approximations typically made in practical DFT calculations, and of some extensions and generalizations of DFT.

It is here where DFT provides a viable alternative, less accurate perhaps, but much more versatile. DFT explicitly recognizes that nonrelativistic Coulomb systems differ only by their potential $v(r)$, and supplies a prescription for dealing with the

universal operators $\hat{T}$ and $\hat{U}$ once and for all. Furthermore, DFT provides a way to systematically map the many-body problem, with $\hat{U}$, onto a single-body problem, without $\hat{U}$. All this is done by promoting the particle density *n(r)* from just one among many observables to the status of key variable, on which the calculation of all other observables can be based. This approach forms the basis of the large majority of electronic-structure calculations in physics and chemistry. Much of what we know about the electrical, magnetic, and structural properties of materials has been calculated using DFT, and the extent to which DFT has contributed to the science of molecules is reflected by the 1998 Nobel Prize in Chemistry, which was awarded to Walter Kohn, the founding father of DFT, and John Pople, who was instrumental in implementing DFT in computational chemistry. The Density Functional approach can be summarized by the sequence.

$$n(r) \Longrightarrow \Psi(r_1,...,r_N) \Longrightarrow v(r) \tag{34}$$

i.e., knowledge of *n(r)* implies knowledge of the wavefunction and the potential, and hence of all other observables. Although this sequence describes the conceptual structure of DFT, it does not really represent what is done in actual applications of it, which typically proceed along rather different lines, and do not make explicit use of many-body wavefunctions. The following sections attempt to explain both the conceptual structure and some of the many possible shapes and disguises under which this structure appears in applications.

The Hohenberg-Kohn theorem

At the heart of DFT is the Hohenberg-Kohn (HK) theorem. This theorem states that for ground states equation (34) can be inverted: given a ground state density $n_0(r)$ it is possible, in principle, to calculate the corresponding ground-state wavefunction $\Psi_0(r_1, r_2,...,r_N)$. This means that Ψ_0 is a functional of n_0. Consequently, all ground-state observables are functionals of n_0, too. If Ψ_0 can be

calculated from n_0 and vice versa, both functions are equivalent and contain exactly the same information. At first sight this seems impossible: how can a function of one (vectorial) variable r be equivalent to a function of N (vectorial) variables $r_1 \ldots r_N$? How can one arbitrary variable contain the same information as N arbitrary variables?

The crucial fact which makes this possible is that knowledge of $n_0(r)$ implies implicit knowledge of much more than that of an arbitrary function $f(r)$. The ground-state wavefunction ψ_0 must not only reproduce the ground-state density, but also minimize the energy. For a given ground-state density $n_0(r)$, we can write this requirement as

$$E_{v,0} = \min_{\Psi \to n_0} < \Psi \mid \hat{T} + \hat{U} + \hat{V} \mid \Psi > \qquad (35)$$

where $E_{v,0}$ denotes the ground-state energy in potential $v(r)$. The preceding equation tells us that for a given density $n_0(r)$ the ground-state wavefunction ψ_0 is that which reproduces this $n_0(r)$ and minimizes the energy.

For an arbitrary density $n(r)$, we define the functional

$$E_v[n] = \min_{\Psi \to n} < \Psi \mid \hat{T} + \hat{U} + \hat{V} \mid \Psi > \qquad (36)$$

If n is a density different from the ground-state density n_0 in potential $v(r)$, then the ψ that produce this n are different from the ground-state wavefunction ψ_0, and according to the variational principle the minimum obtained from $E_v[n]$ is higher than (or equal to) the ground-state energy $E_{v,0} = E_v[n_0]$. Thus, the functional $E_v[n]$ is minimized by the ground-state density n_0, and its value at the minimum is $E_{v,0}$.

The total-energy functional can be written as

$$E_v[n] = \min_{\Psi \to n} < \Psi \mid \hat{T} + \hat{U} \mid \Psi > + \int d^3 r n(r) v(r) = F[n] + V[n] \qquad (37)$$

where the internal-energy functional $F[n] = \min_{\Psi \to n} < \Psi | \hat{T} + \hat{U} | \Psi >$ (universal functionals) is independent of the potential *v(r)*, and thus determined only by the structure of the operators $\hat{U}$ and $\hat{T}$. This universality of the internal-energy functional allows us to define the ground-state wavefunction ψ_0 as that antisymmetric *N*-particle function that delivers the minimum of *F[n]* and reproduces n_0. If the ground state is nondegenerate, this double requirement uniquely determines ψ_0 in terms of $n_0(r)$, without having to specify *v(r)* explicitly.

Equations (35) to (37) constitute the constrained search proof of the Hohenberg-Kohn theorem. The original proof by Hohenberg and Kohn proceeded by assuming that ψ_0 was not determined uniquely by n_0 and showed that this produced a contradiction to the variational principle. Both proofs, by constrained search and by contradiction, are elegant and simple. In fact, it is a bit surprising that it took 38 years from Schrödinger's first paper on quantum mechanics to Hohenberg and Kohn's 1964 paper containing their famous theorem. Since 1964, the HK theorem has been thoroughly scrutinized, and several alternative proofs have been found. One of these is the so-called 'strong form of the Hohenberg-Kohn theorem', based on the inequality.

$$\int d^3 r \Delta n(r) \Delta v(r) < 0 \qquad (38)$$

Here $\Delta v(r)$ is a change in the potential, and $\Delta n(r)$ is the resulting change in the density. We see immediately that if $\Delta v \neq 0$ we cannot have $\Delta n(r) \equiv 0$, i.e., a change in the potential must also change the density. This observation implies again the HK theorem for a single density variable: there cannot be two local potentials with the same ground-state charge density. A given-particle ground-state density thus determines uniquely the corresponding potential, and hence also the wavefunction. Moreover, equation (38) establishes a relation between the signs of $\Delta n(r)$ and $\Delta v(r)$: if Δv is mostly positive, $\Delta n(r)$ must be mostly negative, so that their integral over all space is negative. This additional information is not immediately available from the

two classic proofs, and is the reason why this is called the 'strong' form of the HK theorem. Equation (38) can be obtained along the lines of the standard HK proof, but it can be turned into an independent proof of the HK theorem because it can also be derived perturbatively.

Another alternative argument is valid only for Coulomb potentials. It is based on Kato's theorem, which states that for such potentials the electron density has a cusp at the position of the nuclei, where it satisfies

$$Z_k = -\frac{a_0}{2n(r)} \left.\frac{dn(r)}{dr}\right|_{r->R_k} \tag{39}$$

Here R_k denotes the positions of the nuclei, Z_k their atomic number, and $a_0 = \dfrac{\hbar^2}{2me}$ is the Bohr radius. For a Coulomb system one can thus, in principle, read off all information necessary for completely specifying the Hamiltonian directly from examining the density distribution: the integral over $n(r)$ yields N, the total particle number; the position of the cusps of $n(r)$ are the positions of the nuclei, R_k; and the derivative of $n(r)$ at these positions yields Z_k by means of equation (39). This is all one needs to specify the complete Hamiltonian of equation (and thus implicitly all its eigenstates). In practice one almost never knows the density distribution sufficiently well to implement the search for the cusps and calculate the local derivatives. Still, Kato's theorem provides a vivid illustration of how the density can indeed contain sufficient information to completely specify a nontrivial Hamiltonian.

The Kohn-Sham Equations

Density Functional Theory can be implemented in many ways. The minimization of an explicit energy functional, discussed up to this point, is not normally the most efficient among them. Much more widely used is the Kohn- Sham approach. Interestingly, this approach owes its success and popularity partly to the fact that it does not exclusively work in terms of the particle (or charge) density, but

brings a special kind of wavefunctions (single-particle orbitals) back into the game. As a consequence DFT then looks formally like a single-particle theory, although many-body effects are still included via the so-called exchange-correlation functional. We will now see in some detail how this is done.

Exchange-correlation energy

The Thomas-Fermi approximation for $T[n]$ is not very good. A more accurate scheme for treating the kinetic-energy functional of interacting electrons, $T[n]$, is based on decomposing it into one part that represents the kinetic energy of noninteracting particles of density n, i.e., the quantity called above $T_s[n]$, and one that represents the remainder, denoted $T_c[n]$ (the sub-scripts s and c stand for 'single-particle' and 'correlation', respectively).

$$T[n] = T_s[n] + T_c[n] \qquad (40)$$

$T_s[n]$ is not known exactly as a functional of n, but it is easily expressed in terms of the single-particle orbitals $\varphi i(r)$ of a noninteracting system with density n, as

$$T_s[n] = -\frac{\hbar^2}{2m} \sum_i^N \int d^3r \phi_i^*(r) \nabla^2 \phi_i(r) \qquad (41)$$

because for noninteracting particles the total kinetic energy is just the sum of the individual kinetic energies. Since all $\varphi i(r)$ are functionals of n, this expression for T_s is an explicit orbital functional but an implicit density functional, $T_s[n] = T_s[\{\varphi_i[n]\}]$, where the notation indicates that T_s depends on the full set of occupied orbitals φ_i, each of which is a functional of n. Other such orbital functionals will be discussed later.

We now rewrite the exact energy functional as

$$E[n] = T[n] + U[n] + V[n] = T_s\left[\{\phi_i[n]\}\right] + U_H[n] + E_{xc}[n] + V[n] \qquad (42)$$

where by definition E_{xc} contains the differences $T - T_s$ (i.e. T_c) and $U - U_H$. This definition shows that a significant part of the correlation energy E_c is due to the difference T_c between the noninteracting and the interacting kinetic energies. Equation (42) is formally exact, but of course E_{xc} is unknown — although the HK theorem guarantees that it is a density functional. This functional, $E_{xc}[n]$, is called the exchange-correlation (*xc*) energy. It is often decomposed as $E_{xc} = E_x + E_c$, where E_x is due to the Pauli principle (exchange energy) and E_c is due to correlations. (T_c is then a part of E_c.) The exchange energy can be written explicitly in terms of the single-particle orbitals as

$$E_x[\{\phi_i[n]\}] = -\frac{q^2}{2} \sum_{jk} \int d^3r \int d^3r' \int \frac{\phi_i^*(r)\phi_k^*(r)\phi_j(r')\phi_k(r)}{|r-r'|} \tag{43}$$

which is known as the Fock term, but no general exact expression in terms of the density is known.

There are basically three distinct types of approximations involved in a DFT calculation. One is conceptual, and concerns the interpretation of KS eigenvalues and orbitals as physical energies and wavefunctions. The second type of approximation is numerical, and concerns methods for actually solving the differential equation. A main aspect here is the selection of suitable basis functions. The third type of approximation involves constructing an expression for the unknown *xc* functional $E_{xc}[n]$, which contains all many-body aspects of the problem. It is with this type of approximation that we are concerned in the present section. This part is intended to give the reader an idea of what types of functionals exist, and to describe what their main features are, separately for local functionals (TF, LDA and Xα), semilocal, or gradient dependent functionals (GEA and GGA), and nonlocal functionals (hybrids, orbital functionals such as meta-GGAs, EXX and SIC, and integral dependent functionals such as ADA). This chapter does deal only most superficially with the actual construction of these functionals.

Local functionals: LDA

Historically (and in many applications also practically) the most important type of approximation is the local-density approximation (LDA). To understand the concept of an LDA recall first how the noninteracting kinetic energy $T_s[n]$ is treated in the Thomas-Fermi approximation: In a homogeneous system one knows that,

$$t_s^{hom}(n) = \frac{3\hbar^2}{10m}(3\pi^2)^{2/3}n^{5/3} \tag{44}$$

where $n = const.$ In an inhomogeneous system, with $n = n(r)$, one approximates locally

$$t_s(r) \approx t_s^{hom}(n(r)) = \frac{3\hbar^2}{10m}(3\pi^2)^{2/3}n(r)^{5/3} \tag{45}$$

and obtains the full kinetic energy by integration over all space

$$T_s^{LDA}[n] = \int d^3r\, t_s^{hom}(n(r)) = \frac{3\hbar^2}{10m}(3\pi^2)^{2/3}\int d^3r\, n(r)^{5/3} \tag{46}$$

For the kinetic energy the approximation $T_s[n] \approx T_s^{LDA}[n]$ is much inferior to the exact treatment of T_s in terms of orbitals, offered by the Kohn-Sham equations, but the LDA concept turns out to be highly useful for another component of the total energy, the exchange-correlation energy $E_{xc}[n]$. For the exchange energy $E_x[n]$ the procedure is very simple, since the per volume exchange energy of the homogeneous electron liquid is known exactly

$$e_x^{hom}(n) = -\frac{3q^2}{4}(\frac{3}{\pi})^{1/3}n^{4/3} \tag{47}$$

so that

$$E_x^{LDA}[n] = -\frac{3q^2}{4}(\frac{3}{\pi})^{1/3}\int d^3rn(r)^{4/3} \qquad . \qquad (48)$$

This is the LDA for E_x

For the correlation energy $E_c[n]$ the situation is more complicated since $e_c^{hom}(n)$ is not known exactly: the determination of the correlation energy of a homogeneous interacting electron system (an electron liquid) is already a difficult many-body problem on its own! Early approximate expressions for $e_c^{hom}(n)$ were based on applying perturbation theory (e.g. the random phase approximation) to this problem. These approximations became outdated with the advent of highly precise Quantum Monte Carlo (QMC) calculations for the electron liquid, by Ceperley and Alder. Modern expressions for $e_c^{hom}(n)$ are parameterizations of these data. These expressions are implemented in most standard DFT program packages and in typical applications give almost identical results. On the other hand, the earlier parameterizations of the LDA, based on perturbation theory, can occasionally deviate substantially from the QMC ones, and are better avoided. Independently of the parameterizations, the LDA for $E_{xc}[n]$ formally consists in

$$E_{xc}[n] \approx E_{xc}^{LDA}[n] = \int d^3r e_{xc}^{hom}(n)|_{n->n(r)} = \int d^3r e_{xc}^{hom}(n(r)) \qquad (49)$$

where $e_{xc}^{hom} = e_x^{hom} + e_c^{hom}$. The corresponding xc potential is simply

$$v_{xc}^{LDA}[n](r) = \frac{\partial e_{xc}^{hom}(n)}{\partial n}\bigg|_{n->n(r)} \qquad (50)$$

For many decades the LDA has been applied in, e.g., calculations of band structures and total energies in solid-state physics. In quantum chemistry it is much less popular, because it fails to provide results that are accurate enough to permit a quantitative discussion of the chemical bond in molecules (so-called 'chemical accuracy' requires

calculations with an error of not more than about 1 kcal/mol = 0.04336 eV/particle).
At this stage it may be worthwhile to recapitulate what practical DFT does, and where
the LDA enters its conceptual structure: What real systems, such as atoms, molecules,
clusters and solids, have in common, is that they are simultaneously inhomogeneous
(the electrons are exposed to spatially varying electric fields produced by the nuclei)
and interacting (the electrons interact via the Coulomb interaction). The way density-
functional theory, in the local-density approximation, deals with this inhomogeneous
many-body problem is by decomposing it into two simpler (but still highly nontrivial)
problems: the solution of a spatially homogeneous interacting problem (the
homogeneous electron liquid) yields the uniform *xc* energy $e_c^{\text{hom}}(n)$ and the solution of
a spatially inhomogeneous noninteracting problem (the inhomogeneous electron gas
described by the KS equations) yields the particle density. Both steps are connected
by the local-density potential (50), which shows how the *xc* energy of the uniform
interacting system enters the equations for the inhomogeneous noninteracting system.
The particular way in which the inhomogeneous many-body problem is decomposed,
and the various possible improvements on the LDA, is behind the success of DFT in
practical applications of quantum mechanics to real materials. Some such
improvements on the LDA are discussed in the next two sections.

Semilocal functionals: GEA, GGA and beyond

In the LDA one exploits knowledge of the density at point r. Any real system
is spatially inhomogeneous, i.e., it has a spatially varying density *n(r),* and it would
clearly be useful to also include information on the rate of this variation in the
functional. A first attempt at doing this was the so-called 'gradient-expansion
approximations' (GEA). In this class of approximation one tries to systematically
calculate gradient-corrections of the form $|\Delta n(r)|$, $|\Delta n(r)|^2$, $\Delta^2 n(r)$, etc., to the LDA. A
famous example is the lowest-order gradient correction to the Thomas-Fermi
approximation for *T_s[n],*

$$T_s[n] \approx T_s^W[n] = T_s^{LDA}[n] + \frac{\hbar^2}{8m} \int d^3r \frac{|\nabla n(r)|^2}{n(r)} \qquad (51)$$

This second term on the right-hand side is called the Weizsacker term. Similarly, in

$$E_x[n] \approx E_x^{GEA(2)}[n] = E_x^{LDA}[n] - \frac{10q^2}{432\pi(3\pi^2)^{1/3}} \int d^3r \frac{|\nabla n(r)|^2}{n(r)^{4/3}} \qquad (52)$$

the second term on the right-hand side is the lowest-order gradient correction to $E_x^{LDA}[n]$. In practice, the inclusion of low-order gradient corrections almost never improves on the LDA, and often even worsens it. Higher-order corrections (e.g., $\alpha|\nabla n(r)|^\alpha$ or $\beta \nabla^\beta n(r)$ with $\alpha, \beta > 2$), on the other hand, are exceedingly difficult to calculate, and little is known about them. In this situation it was a major breakthrough when it was realized, in the early eighties, that instead of power-series-like systematic gradient expansions one could experiment with more general functions of *n(r)* and $\nabla n(r)$, which need not proceed order by order. Such functionals, of the general form

$$E_{xc}^{GGA}[n] = \int d^3r f(n(r), \nabla n(r)) \qquad (53)$$

have become known as generalized-gradient approximations (GGAs)

Different GGAs differ in the choice of the function *f(n, ∇ n)*. Note that this makes different GGAs much more different from each other than the different parameterizations of the LDA: essentially there is only one correct expression for $e_{xc}^{hom}[n]$, and the various parameterizations of the are merely different ways of writing it. On the other hand, depending on the method of construction employed for obtaining *f(n, ∇ n)* one can obtain very different GGAs. In particular, GGAs used in quantum chemistry typically proceed by fitting parameters to test sets of selected molecules. On the other hand, GGAs used in physics tend to emphasize exact constraints. Nowadays the most popular (and most reliable) GGAs are PBE (denoting the functional proposed in 1996 by Perdew, Burke and Ernzerhof (Perdew *et al.*,

1997)) in physics, and BLYP (denoting the combination of Becke's 1988 exchange functional (Becke *et al.*, 1988) with the 1988 correlation functional of Lee, Yang and Parr (Lee *et al.*, 1988)) in chemistry. Many other GGA-type functionals are also available, and new ones continue to appear. Quite generally, current GGAs seem to give reliable results for all main types of chemical bonds (covalent, ionic, metallic and hydrogen bridge). For van der waals interactions, however, common GGAs and LDA fail. To describe these very weak interactions several more specialized approaches have been developed within DFT. Both in physics and in chemistry the widespread use of GGAs has lead to major improvements as compared to LDA. 'Chemical accuracy', as defined above, has not yet been attained, but is not too far away either.

The hybrid method

In spite of these advances, the quest for more accurate functionals goes ever on, and both in chemistry and physics various beyond-GGA functionals have appeared. Perhaps the most popular functional in quantum chemistry is B3LYP. This is a combination of the LYP GGA for correlation (Lee *et al.*, 1988) with Becke's three-parameter hybrid functional B3 for exchange (Becke *et al.*, 1988). Common hybrid functionals, such as B3, mix a fraction of Hartree-Fock exchange into the DFT exchange functional (other mixtures are also possible). The construction of hybrid functional involves a certain amount of empiricism in the choice of functionals that are mixed and in the optimization of the weight factors given to the HF and DFT terms. Formally, this might be considered a drawback, but in practice B3 has proven to be the most successful exchange functional for chemical applications, in particular when combined with the LYP GGA functional for E_c. More extreme examples of this semiempirical mode of construction of functionals are Becke's 1997 hybrid functional (Becke *et al.,* 1997)

CURRICULUM VITAE

PERSONAL DATA

Name: Miss Panvika Pannopard

Date of birth: June 9, 1980

Place of birth: Bangkok, Thailand

Nationallity: Thai

EDUCATION

: YEAR	INSTITUTION	DEGREE
1997-2001	Thammasart University	B.Sc. (Chemistry)

SCHOLARSHIP: Scholarships from the Postgraduate on Education and research in Petroleum and Petrochemical Technology (ADB-MUA) (2004-2005)